# COMPUTATIONAL MODELING OF THROMBUS FORMATION IN A SIMPLE ARTERY MODEL

by

Ge Yan

A thesis submitted to Johns Hopkins University in conformity with the requirements for the degree of Master of Science in Engineering

Baltimore, Maryland
May, 2017

# Abstract

The present study focuses on the numerical investigation of thrombus formation in a modeled artery, and in particular, on the validation of a coupled chemo-fluidic computational model for thrombus formation via comparison with the experimental results. In a series of simulations, a backward-facing step (BFS) in a circular pipe, which models an abnormal vessel, is adopted to generate a flow with large-scale separation, which creates conditions for thrombus formation. The modeled thrombus formation process - coagulation cascade and platelet aggregation are solved together with the incompressible Navier-Stokes equations for the blood flow dynamics, in which the blood is treated as a Newtonian fluid. The simulation set up matches the experiment reported in the literature and the simulation results are compared to the experimental ones. Metrics associated with the thrombus formation such as the concentration of tissue factor, thrombin, activated platelets, and fibrin as well as the residence time, are quantified. Moreover, based on the difference between the results from the simulations and the experimental data, several undetermined parameters controlling platelet activation and adhesion are explored. In this study, the chemo-fluidic computational model is extended by including the effects of thrombus on the flow and thus the flow and thrombus dynamics are modeled in a two-way coupled manner. The results of this two-way coupling are also discussed.

## Acknowledgement

First of all, I sincerely thank Dr. Mittal for providing me this opportunity working in his group in the past two years. The experience as a research assistant prepares me for my future Ph.D. research and study. Moreover, I would like to express my gratitude to him for the useful comments, remarks and engagement through the learning process of this master thesis.

Second, I would also thank Dr. Seo for his patience guidance, endless support and heartfelt encouragement. His guidance helped me in all the time of research and writing of this thesis. I could not have imagined having a better advisor and mentor for my Master study. Also my thanks go to my fellow labmates: Chi Zhu and Zhuoyu Zhou, for discussing problems and answering my questions.

Last but not least, I would like to thank my families for their support and understanding. Thank them for supporting me throughout all my studies at Johns Hopkins University.

# Table of Contents

# List of Figure

# List of Table

# Introduction

Thrombosis in the cardiovascular system can lead to critical events associated with myocardial infarction (MI) and stroke, and thromboembolic disorders account for considerable overall morbidity and mortality. Stroke is a major source of mortality and morbidity in US society and one quarter of the 795,000 strokes occur each year are recurrent events1). Thromboembolism is one of the major causes of stroke, especially cardiogenic cerebral embolism is responsible for approximately 20% of ischemic strokes. Left ventricular thrombus (LVT) formed after acute myocardial infarction (AMI) can detach from the damaged endothelium and travel to the cerebrovascular system causing stroke event. Moreover, venous thrombii are the second leading cause of death in patients with cancer4).

In order to prevent thrombosis in the cardiovascular system and resulting thromboembolic events, anti-thrombotic therapy can be applied. Effective therapies for thromboembolism are, however, not free from risk. For example, “triple therapy” in patients with ST elevation MI increases fatal and non-fatal bleeding risk over 20% up to 90 days5). To minimize the bleeding risk, a reliable risk stratification method is therefore required. Current stratification of patient risk for LVT formation is based on general information about the LV and its lack of sensitivity and specificity makes it an unreliable approach for stratification of LVT risk. To develop more reliable risk stratification methods, we may need a better understanding on the interaction between the blood flow and the biochemistry of thrombus formation. Computational modeling provides the possibility of providing detailed insights in to this interaction. Such a model should take account of factors including blood flow patterns, biochemical reactions, and geometry. A more accurate stratification can be proposed based on the insight obtained from the simulation results and it could

also eventually help determine the management of associated disease conditions.

Recently, a chemo-fluidic coupled computational model has been proposed by Seo et al.5) to investigate = thrombus formation process in the LV. The advantage of this computational model is that the hemodynamic flow and the biochemical reactions associated with thrombus formation are solved together and can be tracked simultaneously. This model has been applied to canonical 5) as well as patient-specific 22) cases, and based on the simulation results, a new metric for the LVT risk is proposed5). This is a good example of the role that computational modeling and associated analysis can play in the development of new diagnostic methods. The chemo-fluidic computational model itself, however, contains many parameters and has not yet been validated against in-vitro experiments. In the present study, this model is applied to a relatively simple geometry where the bench-top experimental results are available, and the simulation results are compared with the experimental ones to validate the model.

## Thrombosis

Thrombosis happens when pathologic processes overwhelm the dynamic equilibrium associated with hemostasis. The hemostasis process is responsible for reestablishing the integrity of the tissue after vascular damage. However, blood clots or “thrombi”, which are structures made of a fibrin mesh, activated platelets and other cells, and thrombi in arteries and veins can grow up to large sizes that can occlude the vessel. . Thrombosis involves two interactive process: platelet coagulation and aggregation, in which the coagulation is a cascade of biochemical reactions that generate the constituents of the clot and the aggregation is the mostly physical process that makes platelets clump together adhere to the wall. Tissue factor initiates the blood coagulation process,

which culminates in the generation of thrombin and fibrin 4)6). Thrombin activates platelets, which then aggregate at the site of the injury and become the main component of the thrombus; Both processes are largely controlled by the flow pattern in the given geometry and in turn, as thrombus concentration grows it exerts frictional resistance slowing down the surrounding blood flow and accelerating coagulation and aggregation processes. Finally, the thrombus size will reach a dynamic equilibrium under the influence of resistance force and its "counterpart" wall shear rate.

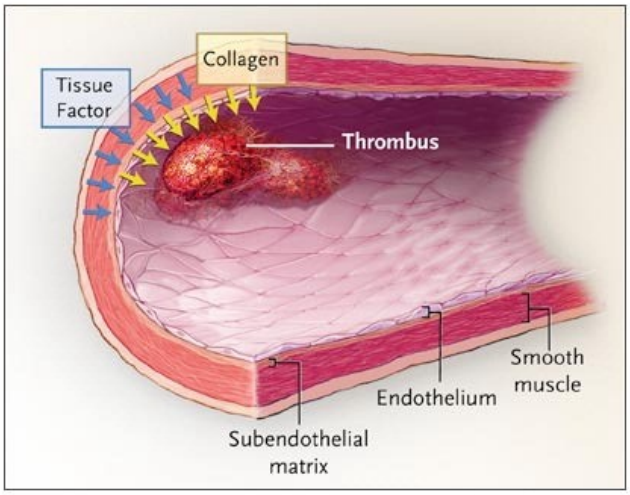


Figure 1 Response to vascular injury - mechanism of platelets activation[4].

There are two independent pathways that can initiate the thrombus formation: exposure of sub endothelial collagen which leads to platelets activation and initiation via thrombin generated by tissue factor (TF) 4). For the former, the interactions between platelet glycoprotein VI results in adhesion of platelets to the site of injury, in which platelet glycoprotein VI also acts as the major agonist for platelet activation and granule release. Platelet activation initiated by TF doesn't require disruption of the endothelium and is independent of von Willebrand 7) Factor (vWF) and platelet glycoprotein8).

The coagulation cascade starts with activation of encrypted TF by protein disulfide isomerase on the exposed subendothelium and process with other enzyme reactions4)6). Thrombin, a major product of cascade reaction, is critical in the reaction series since it (1) accelerates its own production rate by affecting early reactions, (2) activates platelets, and (3) transfers soluble plasma protein fibrinogen to insoluble fibrin, which eventually forms fibrin mesh mixed with platelet thrombus.

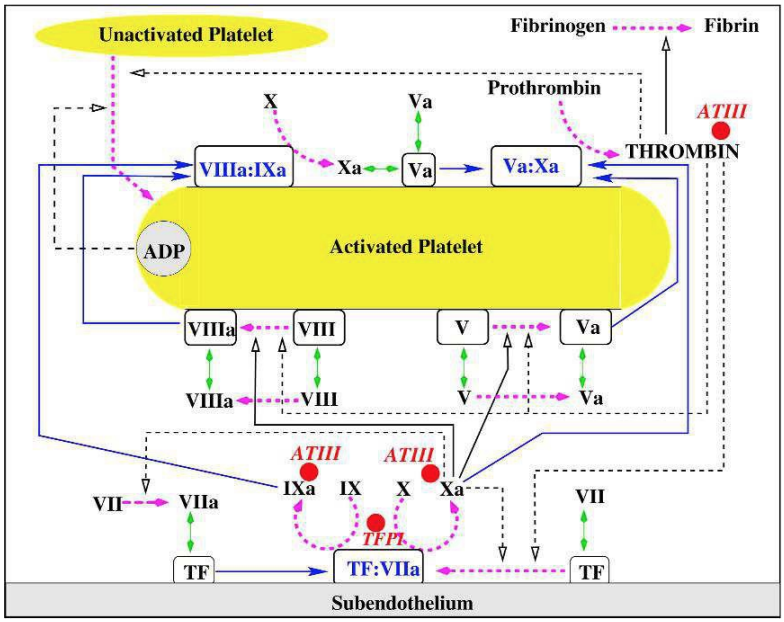


Figure 2 A schematic of the coagulation cascade including species and reactions. The dashed magenta arrows represent activation processes, blue arrows represent chemical transport, green segments represent surface binding/unbinding, solid black lines represent f forward enzyme action, dashed black lines show enzyme feedback, and red disks represent chemical inhibitors 6).

This study uses the following abbreviations to outline the essential reactions in coagulation cascade: TF for tissue factor, APC for activated protein C, TFPI for tissue factor pathway inhibitor, ADP for adenosine diphosphate, ATIII for antithrombin-III. Moreover, all the proteins in the cascade have active and inactive forms. The inactive zymogens are VII, IX, X, and II. The active forms of these zymogens are VIIa, IXa, Xa, and IIa respectively. As the injured subendothelium release TF

molecules into the blood flow, the cascade is initiated by the combination of VIIa and TF. Enzymes IXa and Xa activated by complex TF:VIIa can be part of any enzyme complex on the surface of activated platelet. On platelet surface, platelet bounded enzymes Xa also activates Va and VIIIa released from subendothelium. The crucial product in the cascade, thrombin, is activated by prothrombinase (Va:Xa) formed by combination of Xa and platelet bounded Va. Platelets can also be activated by connection with subendothelium or ADP, which is released during the platelet activation 6).

Platelet aggregation refers to the processes where platelets bind to the subendothelium or other activated platelets. The first process is known as platelet adhesion wherein platelet glycoprotein VI interacts with collagen and platelet glycoprotein Ib-V-IX with collagen-bound von Willebrand factor 4). The process where platelets bind to other activated platelets is known as cohesion. In either case, blood flow exerts a drag force that opposes the initial establishment and further growth of thrombus. Thus it can be concluded that the platelet aggregation process is greatly influenced by high wall shear stress (WSS).

## Role of Hemodynamics

Blood flow dynamics plays a crucial role in thrombus formation. Several studies have investigated the fluid mechanics leading to thrombosis, but the mechanisms affecting thrombus formation are still not well understood 10). Thrombus formation seems to be associated with regions where the blood flow rate or its direction change change significantly. In this regard, flow separation, which happens due to significant changes in vessel diameter or curvature provides preferential conditions for thrombus formation. The recirculation region associated with a separated flow provides

increased residence time for platelet activation and platelet deposition. The flow Reynolds number seems to be another crucial factor that influences thrombus formation. In several experimental studies, thrombus formation was observed in a low and narrow range of Reynolds numbers. Moreover, in the experiments done by T. Karino et al. 11) the aggregation process diminishes and then disappears at high Reynolds numbers.

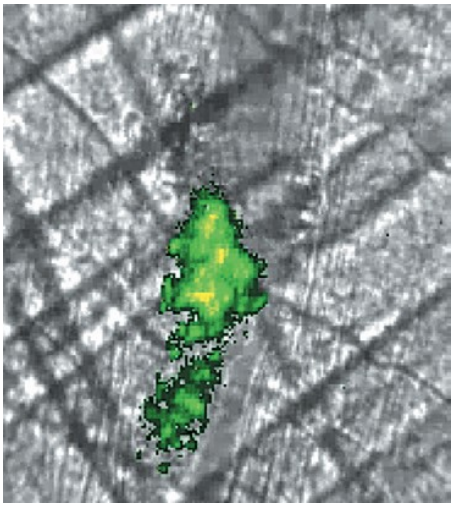

Figure 3 Visualization of platelet in Vivo. Resting platelets show in green and activated platelet in yellow [4].

Hemodynamics also plays an important role in thromboembolic events that result downstream of the thrombus. During thrombus growth, unstimulated platelets might cohere to thrombus surface loosely. Due to the shear stresses induced by the flow, these platelets are likely to disengage from the thrombus. The shape of the thrombus is influenced greatly by the hemodynamics, and finally the architecture of thrombus will reach a dynamic equilibrium due to the balance between thrombus formation and the wall shear stress 4). Moreover, thrombus propagation is not limited to unstimulated platelets. Because of the high shear stress, the thrombus could detach from the subendothelium and travel to other locations in the blood stream. Thrombus detachment can be deadly because it can cause embolic events in the vascular system in which the emboli size is

larger than the vessel diameter. One of the most feared embolism is known as cardiogenic cerebral embolism.

## Computational models

Extensive work has been done on developing computational models of thrombus formation. Leiderman and Fogelson 6) developed a numerical model to simulate spatial-temporal evolution of platelet deposition, in which they adopt and improved the computational model proposed by Kuharsky & Fogelson 21). In the KF model, all the species in the biochemical reactions were assumed to be well-mixed near subendothelium. This "well-mixed" system intrinsically limits this model to be valid near the vessel wall. Leiderman and Fogelson made improvements in the following aspects: 1) use the same assumption for chemical species not only in the near wall region but also into the lumen, 2) couple the chemical reactions with local fluid dynamics, 3) explicitly treat the platelet activating agonist ADP. However, in their study, they only simulate thrombosis in 2D geometry, where the blood flows above damaged vessel walls 6).

Biasetti et al. 13) develop a model based on the coagulation cascade proposed by Jones and Mann 12). Their CC model consists of a total of 18 species, and both the plasma-phase and membrane-phase reactions are considered. TF and factor VIIa are not considered separately but in a joint form TF:VIIa. Because on a local level, the differences of flow pattern between non-Newtonian model and Newtonian model is substantial, which is caused by the blood non-Newtonian properties like shear-shinning, thixotropic, and viscoelasticity, they take the non-Newtonian behavior of blood into proper consideration. For the shear-shinning they adopt the Carreu-Yasuda (CY) model 13).

The experimental and computational studies conducted by Neeves et al. 14) focus primarily on the formation of fibrin and its relationship with wall shear stress and thrombin flux. In their reaction system, there are only thrombin, fibrinogen and reaction product fibrin monomer. The experimental results show that the thickness and shape of fibrin are solely functions of wall shear stress; only concentration of fibrin varies accordingly with thrombin flux. At a constant wall shear stress rate, fibrin decomposition and morphology are largely influenced by thrombin flux.

The study from Seo et al combines the models discussed above. This model is currently the most comprehensive one because it takes fibrin decomposition, coagulation cascade, and platelet activation and aggregation into consideration. Because this study focuses on thrombus formation in the left ventricle, the blood is treated as a Newtonian fluid. The coagulation cascade model is adopted from Biasetti et al. 13) and contains 16 reactions among 18 species. The fibrinogen polymerization model is adopted from Neevas et al. 14). For platelet activation and aggregation, the model is based on the work of Leiderman and Fogelson 6) and categorizes platelets into 3 groups: 1) inactive, mobile platelet, 2) activated, mobile platelets, 3) bound platelets. All the biochemical reactions are solved together with with the incompressible Navier-Stokes equations. 5) More detail about the numerical scheme employed in this model will be discussed later.

## Objective

The objective of this study is the validation of chemo-fluidic computational model using the available bench-top experimental results 15). The computational model from Seo et al 5) is adopted in this study. The benchmark used for comparison is the experiment conducted by Joshua et al. 15). In this experiment thrombus formation in a circular pipe with a backward facing step is studied.

The flow separation generated by the backward facing step is expected to create conditions suitable for thrombus formation. The experiment is conducted at a constant upstream Reynolds number (based on pipe diameter and mean flow velocity) of 490 and the data is collected between 10 and 90 min after the initiation of the flow 15) . Thrombus morphology is measured using Magnetic Resonance Image(MRI) and wall shear stress is calculated using computational fluid dynamics(CFD).

In the current study, the simulation are compared to the experiments results are compared in many aspects: 1) the flow field and circulation area, 2) the general thrombus morphology, 3) the growth rate and distribution of thrombus, thrombin, and TF. Initial simulations employ a one-way coupling between the flow and thrombus where the thrombus does not affect the flow. However, in order to consider the effect of the thrombus on the flow, a penalty force model is included in the second part of the study. Key parameters such as the platelets cohesion and adhesion rates, platelet activation rate, and initial TF condition are varied in the simulations. By comparing the effect of these parameters on the thrombus formation and by validating against the experiments, we hope to develop a better understanding of the capabilities and limits of this models.

# Methods

This section introduces the numerical methods used for our chemo-fluidic coupled computational model and the simulation set up derived from experiment done by Joshua O. et al. The thrombosis model contains three components: 1) the coagulation cascade, 2) platelet activation and adhesion, 3) fibrin formation, which, as pointed earlier, are adopted from three separate studies.

## Hemodynamics

### Governing Equations

In this study, blood flow is treated as a Newtonian fluid and the flow is therefore governed by incompressible Navier-Stokes equations. However, by taking consideration of the effect of thrombus on the blood flow, here we adopt a modified Naver-Stokes equations following Leiderman and Fogleson6):

$$\nabla \cdot \vec{u} = 0, \tag{1}$$

$$\rho\left(\frac{\partial \vec{u}}{\partial t} + \vec{u} \cdot \nabla \vec{u}\right) = -\nabla p + \mu \Delta \vec{u} - \mu \alpha(\phi^B)\vec{u}. \tag{2}$$

Because in this study we are simulating thrombosis in 3D geometry, thus the velocity has three components. $u$ and $p$ are fluid velocity and pressure respectively, and they are functions of time and space; $\rho$ is blood flow density and $\mu$ is dynamic viscosity. The term $\mu\alpha(\phi^B)u$, which is called a Brinkman term, represents the frictional force exerts on the flow by the bound platelets. In this last term, $\phi^B(x,t)$ is the ratio of the sum of bounded platelets number density to the maximum density. The function $\alpha(\phi^B)$ is defined as follow:

$$\alpha(\phi^B) = \alpha_{max}\frac{(\phi^B)^2}{((\phi_0^B)^2 + (\phi^B)^2)}. \tag{3}$$

Because the frictional force is positive relative to the local bounded platelet concentration, function $\alpha(\phi^B)$ increases monotonically with $(\phi^B)$. $\phi_0^B$ indicates the threshold level of bounded platelet where frictional force become significant. The coefficient $\alpha_{max}$ is set to 2000 so that there is almost no flow passing through thrombus when $\phi^B \approx 1$ and in this study, several values for $\phi_0^B$ are used to evaluate the effect of frictional force on thrombus formation.

**Immersed Boundary Method**

In this study, to deal with the geometry of the model, we employ a sharp interface immersed boundary method of Mittal et al. 16) in our simulations. Distinct advantages of this immersed boundary method include: 1) based on calculation of "ghost-cells" inside body, the boundary conditions are satisfied precisely on the immersed boundary, 2) no *ad-hoc* constants and no momentum forcing introduced, 3) interpolation scheme stays well-conditioned and is applied normal to the immersed boundary, 4) successful implementation of same spatial order accuracy with previous cut-cell methods in 3D simulation.

The current immersed boundary method employs a multi-dimensional ghost-cell methodology to impose boundary conditions on arbitrary shaped 2D or 3D immersed stationary and moving boundaries. There are many ways to represent the complex surface in immersed boundary methods. The current solver employs an unstructured mesh with triangular elements. The key to dealing with the complex immersed boundary is to identify the "ghost-cells". Once the unstructured surface mesh is placed in the Cartesian grid, there are cells whose centers are inside the "immersed" boundary but have at least one neighbor in the fluid. Situations can be complicated in 3D due to the arbitrary immersed boundary. Here we show a 2D situation to illustrate the idea.

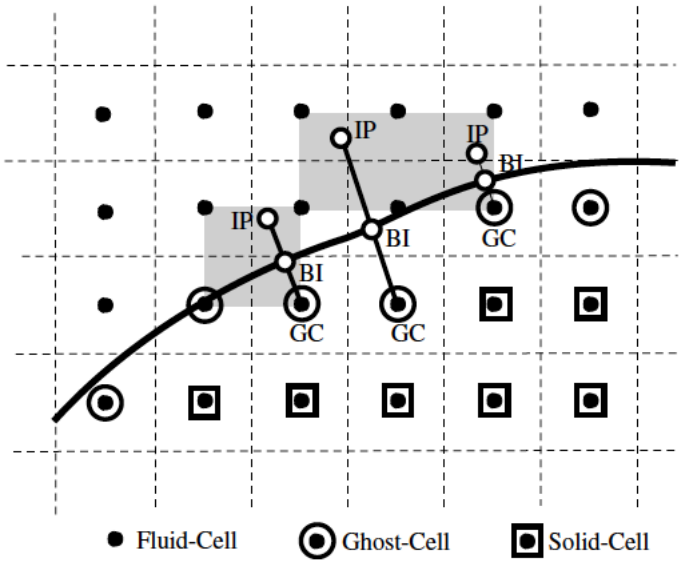


Figure 4 A 2D situation where the immersed boundary cut the Cartesian grid and three different cells are identified in this configuration. BI and IP are boundary intercept and image point respectively [16].

The ghost-cells are those cells whose nodes are located in the first "layer" inside the immersed boundary; fluid cells are cells whose nodes are outside the immersed boundary or occupied by flow; solid-cells are cells entirely inside the stationary or moving body. In order to satisfy the boundary conditions on the immersed boundary in the vicinity of ghost cells, the concept of image point and boundary intercept is introduced. A line segment is extended from ghost cell into fluid to an image point(IP) such that the line segment is normal to the immersed boundary and the boundary intercept (BI) is located at the midpoint for every ghost-cell IP pair. After the identification of IP and BI, any variable of interests (say $\phi$) at IP is calculated by a trilinear interpolation among the eight surrounding nodes of IP:

$$\phi(x_1, x_2, x_3) = C_1 x_1 x_2 x_3 + C_2 x_1 x_2 + C_3 x_2 x_3 + C_4 x_1 x_3 + C_5 x_1 + C_6 x_2 + C_7 x_3 + C_8. \quad (4)$$

The unknown coefficients $C_i$ are also determined by the value of eight surrounding points:

$$\{C\} = [V]^{-1}\{\phi\}, \tag{5}$$

where $[V]$ is the Vandermonde matrix17) and has the form:

$$V = \begin{bmatrix} x_1x_2x_3|_1 & x_1x_2|_1 & \dots x_1|_1 & \dots & 1 \\ x_1x_2x_3|_2 & x_1x_2|_2 & \dots x_1|_2 & \dots & 1 \\ \vdots & \vdots & \dots \ \vdots & \dots & 1 \\ x_1x_2x_3|_8 & x_1x_2|_8 & \dots \ x_1|_8 & \dots & 1 \end{bmatrix}, \tag{6}$$

in which the subscripts are corresponding to the surrounding eight nodes. Finally, the value at IP can be expressed in this form:

$$\phi_{IP} = \sum_{i=1}^{8} \beta_i \phi_i + T.E., \tag{7}$$

where $\beta_i$ is dependent on $C_i$ and IP coordinate, thus $\beta_i$ are determined after the immersed boundary and grid configuration specified. Moreover, the truncation error is said to have order $O(\Delta^2)$ where the grid spacing is $O(\Delta)$. The boundary condition on the immersed boundary is satisfied by using linear approximation of the value at the ghost-cells. For Dirichlet boundary condition (for velocity) on the immersed boundary is satisfied by:

$$\phi_{BI} = \frac{1}{2}(\phi_{IP} + \phi_{GC}) + O(\Delta l^2), \tag{8}$$

where $\Delta l$ is the length of the normal line segment from ghost-cell to IP. By taking previous expression and ignore the truncation error, we have:

$$\phi_{GC} = 2\phi_{BI} - \sum_{i=1}^{8} \beta_i \phi_i. \tag{9}$$

For the pressure Poisson equation, we have Neumann boundary condition on immersed boundary. The expression comes as follow:

$$\left(\frac{\partial \phi}{\partial n}\right)_{BI} = \frac{\phi_{IP} - \phi_{GC}}{\Delta l} + O(\Delta l^2) \tag{10}$$

$$= \frac{1}{\Delta l}\left(\sum_{i=1}^{8} \beta_i \phi_i - \phi_{GC}\right) + O\left(\frac{\Delta^2}{\Delta l}\right) + O(\Delta l^2).$$

The implicit expression of the value for the ghost-cell is:

$$\phi_{GC} - \sum_{i=1}^{8} \beta_i \phi_i = -\Delta l \left(\frac{\partial \phi}{\partial n}\right)_{BI}. \tag{11}$$

Eqs. (9) and (11) are solved together with discretized governing equations. Upon velocity correction, both equations satisfy second order accuracy, which is the same with discretized governing equations.

## Thrombosis Modeling

### Coagulation Cascade

The coagulation cascade model comes from Biasetti et al. 13). Once endothelial damage occurs, the CC is triggered by exposure of extravascular tissue factor (TF) to plasma and subsequent binding with bloodborne factor VIIa, which eventually leads to the formation of thrombin.

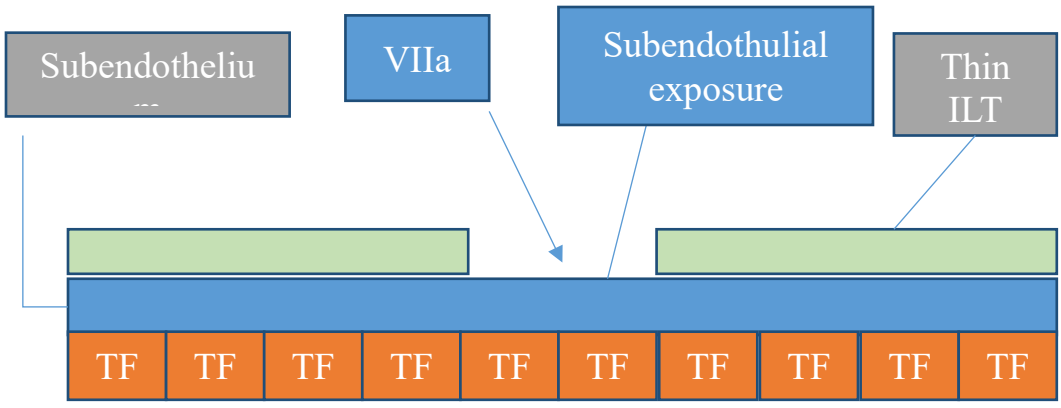


Figure 5 Initial stage of the CC at site of subendothelial exposure.

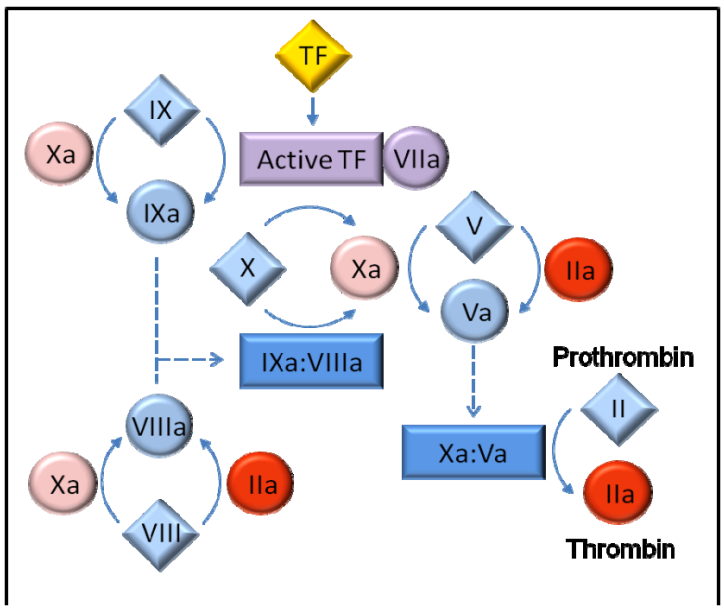


Figure 6 Schematic view of the tissue factor path way of coagulation cascade. TF: tissue factor; Factors VIII, VIIIa, IX, IXa, X, Xa: coagulation factors and their activated forms(a), II, IIa: prothrombin and thrombin.

The CC model contains 18 species, in which enzyme and zymogens are distinguished between active form and inactive form by the subscript "a". The initial concentration of all species is shown in Table 1. The only exception is TF:VIIa, which is set to be 0 at the inlet but 1e-6 at the exposed subendothelium.

Table 1 Initial concentration of the species in the CC model.

| **Species** | **Concentration(mol/m$^3$)** |
|---|---|
| IX | 90E-6 |
| TF:VIIa | 1E-6 |
| X | 170E-6 |
| V | 20E-6 |
| VIII | 0.7E-6 |
| VIIIa | 100E-6 |
| II | 1.4E-6 |
| IX:TF:VIIa | 0 |
| IXa | 0 |
| X:TF:VIIa | 0 |
| X | 0 |

| | |
|---|---|
| VIIIa:IXa | 0 |
| X:VIIIa:IXa | 0 |
| Va | 0 |
| IIa | 0 |
| Va:Xa | 0 |
| II:Va:Xa | 0 |
| mIIa | 0 |

Between the 18 species there are 16 distinctive chemical reactions that are time dependent. These reactions read:

$$\mathrm{IX} + \mathrm{TF{:}\,VIIa} \overset{k_6,k_{16}}{\longleftrightarrow} \mathrm{IX{:}\,TF{:}\,VIIa} \overset{k_{11}}{\longrightarrow} \mathrm{TF{:}\,VIIa} + \mathrm{IXa}, \tag{12}$$

$$\mathrm{X} + \mathrm{TF{:}\,VIIa} \overset{k_6,k_{17}}{\longleftrightarrow} \mathrm{X{:}\,TF{:}\,VIIa} \overset{k_{12}}{\longrightarrow} \mathrm{TF{:}\,VIIa} + \mathrm{Xa}, \tag{13}$$

$$\mathrm{X} + \mathrm{VIIIa{:}\,IXa} \overset{k_6,k_8}{\longleftrightarrow} \mathrm{X{:}\,VIIIa{:}\,IXa} \overset{k_{13}}{\longrightarrow} \mathrm{VIIIa{:}\,IXa} + \mathrm{Xa}, \tag{14}$$

$$\mathrm{IX} + \mathrm{Xa} \overset{k_{15}}{\longrightarrow} \mathrm{Xa} + \mathrm{IXa}, \tag{15}$$

$$\mathrm{V} + \mathrm{Xa} \overset{k_1}{\rightarrow} \mathrm{Xa} + \mathrm{Va}, \tag{16}$$

$$\mathrm{VIII} + \mathrm{Xa} \overset{k_3}{\rightarrow} \mathrm{Xa} + \mathrm{VIIIa}, \tag{17}$$

$$\mathrm{V} + \mathrm{IIa} \overset{k_2}{\rightarrow} \mathrm{IIa} + \mathrm{Va}, \tag{18}$$

$$\mathrm{VIII} + \mathrm{IIa} \overset{k_4}{\rightarrow} \mathrm{IIa} + \mathrm{VIIIa}, \tag{19}$$

$$\mathrm{II} + \mathrm{Va{:}\,Xa} \overset{k_6,k_{19}}{\longleftrightarrow} \mathrm{II{:}\,Va{:}\,Xa} \overset{k_{14}}{\longrightarrow} \mathrm{Va{:}\,Xa} + \mathrm{mIIa}, \tag{20}$$

$$\mathrm{mIIa} + \mathrm{Va{:}\,Xa} \overset{k_5}{\rightarrow} \mathrm{Va{:}\,Xa} + \mathrm{IIa}, \tag{21}$$

$$\mathrm{VIIIa} + \mathrm{IXa} \overset{k_7,k_9}{\longleftrightarrow} \mathrm{VIIIa{:}\,IXa}, \tag{22}$$

$$\mathrm{Va} + \mathrm{Xa} \overset{k_8,k_{10}}{\longleftrightarrow} \mathrm{Va{:}\,Xa}, \tag{23}$$

In these equations, the right-left arrows represent that reactions can go either way. The two coefficients above the arrows represent the rate constant for reaction and its reverse reaction

respectively. Detail information and explanations about the rate constant are given in Table 2.

Table 2 Rate constant used in the CC model.

| | Value | Units | Descriptions |
|---|---|---|---|
| $k_1$ | 2e4 | $mol^{-1}m^3s^{-1}$ | Activation of V by Xa (2nd order) |
| $k_2$ | 2e4 | $mol^{-1}m^3s^{-1}$ | Activation of V by IIa (2nd order) |
| $k_3$ | 1e4 | $mol^{-1}m^3s^{-1}$ | Activation of VIII by Xa (2nd order) |
| $k_4$ | 2e4 | $mol^{-1}m^3s^{-1}$ | Activation of VIII by IIa (2nd order) |
| $k_5$ | 1e4 | $mol^{-1}m^3s^{-1}$ | Conversion of mIIa to IIa by Va:Xa (2nd order) |
| $k_6$ | 1e5 | $mol^{-1}m^3s^{-1}$ | On-rate for rapidly formed complexes (2nd order) |
| $k_7$ | 1e4 | $mol^{-1}m^3s^{-1}$ | On-rate for the VIIIa:IXa complex (2nd order) |
| $k_8$ | 4e5 | $mol^{-1}m^3s^{-1}$ | On-rate for the Va:Xa complex (2nd order) |
| $k_9$ | 0.005 | $s^{-1}$ | Off-rate for VIIIa:IXa complex |
| $k_{10}$ | 0.4 | $s^{-1}$ | Off-rate for Va:Xa complex |
| $k_{11}$ | 0.3 | $s^{-1}$ | Vmax for activation of IX by TF:VIIa |
| $k_{12}$ | 1.15 | $s^{-1}$ | Vmax for activation of X by TF:VIIa |
| $k_{13}$ | 8.2 | $s^{-1}$ | Vmax for activation of IX by VIIIa:IXa |
| $k_{14}$ | 32 | $s^{-1}$ | Vmax for mIIa formation by Va:Xa |
| $k_{15}$ | 1e2 | $mol^{-1}m^3s^{-1}$ | Activation of IX by Xa (2nd order) |
| $k_{16}$ | 24 | $s^{-1}$ | Off-rate for IX on TF:VIIa complex |
| $k_{17}$ | 44 | $s^{-1}$ | Off-rate for X on TF:VIIa complex |
| $k_{18}$ | 0.001 | $s^{-1}$ | Off-rate for X on VIIIa:IXa complex |
| $k_{19}$ | 70 | $s^{-1}$ | Off-rate for II on Va:Xa complex |

Based on the well mixed assumption as well as the notion that all chemical species are carried by blood flow, the chemical concentration can be considered as a function of time. Here we use $c_i(i = 1,2,3 \dots)$ to represent each chemical specie's concentration. Further we solve the convection-diffusion-reaction (CDR) equations to evaluate the chemical concentration at given time and given

location. The equation can be written as:

$$\frac{\partial c_i}{\partial t} + U \cdot \nabla c_i = D_i \nabla^2 c_i + R_i, \tag{24}$$

$U$ is the velocity vector, and $D_i$ is diffusion coefficient for each species. In detail, $D_i$ is set to be equal to $10^{-8} m^2/s$. $R_i$ is the reaction source term is given by

$$R_i = \sum_{j=1}^{16} S_{ij} r_j. \tag{15}$$

$r_j$ is the reaction rate of the j-th reaction, and $S_{ij}$ is the element of stoichiometric matrix $\boldsymbol{S}$ relates to the reactions and species. If i-th specie is presented on the left hand side of j-th reaction, $S_{ij}$ is 1 and -1 if on the right hand side. Otherwise, $S_{ij} = 0$. The reaction rate $r_j$ follow Seo et al. 5).

**Fibrin Formation**

The major product of coagulation cascade, thrombin, also plays an important role in converting fibrinogen into fibrin, which again is a main constituent of the thrombus. This study employs the model from Leiderman et al. 14) which considers a purified system with fibrinogen and thrombin. Furthermore, the fibrin concentration in this model is a function of time and wall shear stress. The equations for non-dimensionalized thrombin $c_t$, fibrinogen $c_f$, and fibrin monomer $c_m$ read:

$$\frac{\partial c_f}{\partial t} + (\vec{U} \cdot \nabla) c_f = D \nabla^2 c_f - k_t c_f, \tag{}$$

$$\frac{\partial c_m}{\partial t} + \overrightarrow{(U} \cdot \nabla) c_m = D \nabla^2 c_m + k_t c_f + k_p c_m^2, \tag{25}$$

in which $k_t$ is the conversion rate defined by:

$$k_t = \frac{k_{cat} c_t}{K_m + c_f}, \tag{26}$$

where $k_{cat} = 84 s^{-1}$, $K_m = 7.2e-3 mol/m^3$, and $k_p = 8.2e2 (mol/m^3)^{-1} s^{-1}$.

**Platelet adhesion and cohesion**

Platelets activation may be initiated by thrombin, exposure to subendothelium, or ADP. In this study, the model we use is a modified version of Leiderman and Fogelson's 6) proposed by Seo et al.5). Platelets are divided into three groups: 1) inactivated, mobile platelets, 2) activated, mobile platelets, and 3) bounded platelets. The equations are slightly modified from original ones and read:

$$\frac{\partial PT_{m,u}}{\partial t} + (U \cdot \nabla)PT_{m,u} = D_p \nabla^2 PT_{m,u} - A_{IIa} PT_{m,u}, \tag{27}$$

$$\frac{\partial PT_{m,a}}{\partial t} + (U \cdot \nabla)PT_{m,a} = D_p \nabla^2 PT_{m,a} + A_{IIa} PT_{m,u} - k_{adh} \cdot h(\vec{x}) \frac{PT_{max} - PT_b}{PT_{max}} PT_{m,a} - k_{coh} \cdot \frac{g(PT_b)}{PT_{max}} PT_{m,a}, \tag{28}$$

$$\frac{\partial PT_b}{\partial t} = k_{adh} h(\vec{x}) \frac{PT_{max} - PT_b}{PT_{max}} PT_{m,a} + k_{coh} \cdot \frac{g(PT_b)}{PT_{max}} PT_{m,a}, \tag{29}$$

in which $PT_{m,u}$, $PT_{m,a}$, and $PT_b$ are inactivated, activated and bounded platelet respectively. Following Leiderman and Fogelson 6), $PT_{max}$ is a constant equals to $6.67e7\ mm^{-3}$ which represents the possible maximum concentration of platelet. The diffusion coefficient $D_p$ is set to $1e-7\ m^2/sec$. $A_{IIa}$ is the platelets activation rate because of thrombin and is defined as:

$$A_{IIa} = \frac{k_u C_{IIa}}{K_{IIa} + C_{IIa}}, \tag{30}$$

in which $k_u = 0.5 sec^{-1}$ and $K_{IIa} = 1e-6\ mol/m^3$. In Eq.(19), the third and forth terms on the right hand side are the sink terms corresponding to adhesion of activated platelet to damaged wall and to bounded platelet respectively. Moreover, these terms are source terms on the right hand side of Eq.20. The function $h(\vec{x})$ is a function indicating the proximity to the damaged wall, and it has value 1 near (within 0.5mm) to the wall and 0 otherwise. The function $g(PT_b)$ is used for calculating the number density of bounded platelet within one computational grid and it is defined

as:

$$g(PT_b)(i,j,k) = \sum_{i_p=-1}^{1} \sum_{j_p=-1}^{1} \sum_{k_p=-1}^{1} PT_b\big(i+i_p, j+j_p, k+k_p\big), \tag{31}$$

where $i, j, k$ are grid indices. We note that the values of the coefficients $k_{adh}$ and $k_{coh}$ are not known and we set them to $5000\ sec^{-1}$ in the current simulations.

**Penalty Force Model**

The penalty forced model is inspired by the fact that the growing thrombus is a porous media through which the blood flow passing at a velocity much less than the main flow. As the thrombus grows and occludes more volume in the vessel, the pressure at the front edge of thrombus will increase, leading to an increase of flow velocity inside the thrombus 6). Initially the velocity within the thrombus increases to the magnitude of $1{\sim}3\ \mu m\ s^{-1}$, leading to advection of fluid-phase chemicals. At later stages due to increased thrombus density, the velocity within thrombus decreases. Because of the porous nature of the growing thrombus, activated platelets may get incorporate into the thrombus. As the thrombus grows, locally thrombus density increases therefore restricting flow and chemicals from entering, which is apparent at 60s in their simulation. To quantitatively account the influence of flow resistance, we introduce a the term $-\mu\alpha(\phi^B)u$ into the Naver-Strokes equation, which is proportional to the bounded platelets density. This term works when bounded platelets density reaches a certain level, which is adjusted in our simulations. The modified equation also indicates that when thrombus density reaches 1, there is no flow pass through the thrombus, which is illustrated in section 2.1.

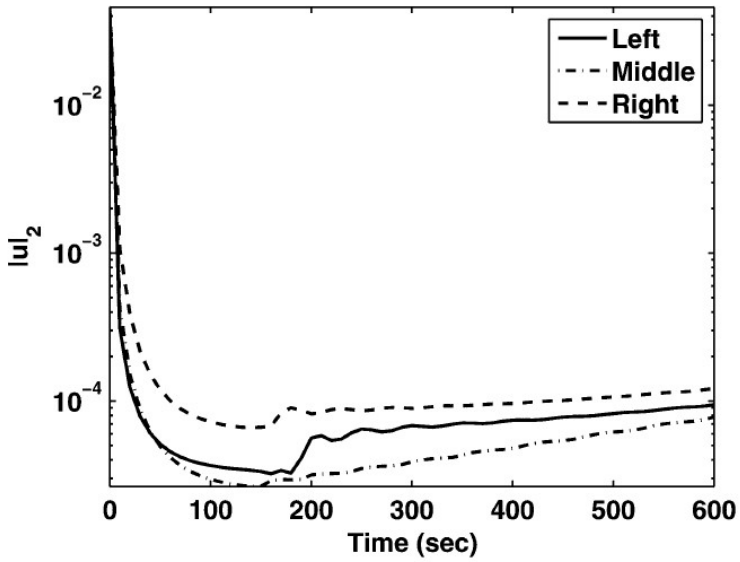


Figure 7 Simulation results from Leiderman and Fogelson. Measurement of velocity in thrombus at 1 μm from the vessel wall. The "Left", "Middle" and "Right" represents the velocity curves at 8 μm from the thrombus left edge, at the middle and the downstream edge.

## Summary of experimental results

As mentioned before, the main purpose of this study is computational model validation with the in-vitro thrombosis experiment done by Joshua et al 15). This section summarizes the experiment set up, procedure, methods and result.

In the experiment, the thrombus formation is studied within a backward facing step (BFS) in the circular pipe. The sudden expansion in BFS model will produce flow separation and thrombus formation is observed in recirculation area 18)19)20). During the experiment, magnetic resonance imaging (MRI) is used to obtain topographic data and measure thrombus size between 10 min to 90 min. Wall shear stress (WSS) distribution on thrombus surface is calculated and correlation between WSS and topography is found. Finally, the study found that the reattachment length is the

best predictor of the thrombus size and volume. The experiment is done in an acrylic BFS model and the experiment set up is shown in figure below.

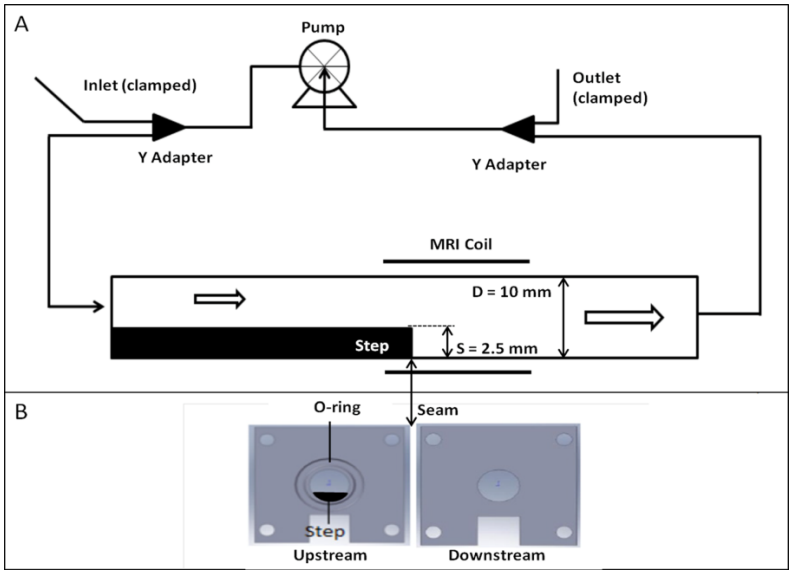


Figure 8 (a) A schematic flow loop set up where arrow indicates the flow direction. (b) The cross sections of BFS inlet and outlet.

The step height is 2.5 mm(S) which is one quarter of down stream vessel diameter, 10 mm(D). The total length of vessel is 40D(400mm) and the step is located at the middle such that the influence of inlet and out let is minimized. Bovine blood is circulated by a peristaltic pump (Cole-Parmer, Vernon Hills, IL, USA) and a 4.0 m long tube is used to connect the whole system, in which the pulsatility inherent to the pump is damped. The average upstream velocity is 0.2m/s and the Reynolds number based on the inlet diameter is 490. The simulation accompanying these experiments is done in BFS geometry without thrombus, and the recirculation area is visualized by stream wise velocity contour (Figure 9). The study found that the best predictor of asymptotic thrombus size is the reattachment length. A series of simulations were done in the presence of different stages of thrombus, which were measures by MRI. The mean WSS, which is calculated on the thrombus surface, is found to be independent of thrombus size, while the maximum WSS is proportional to the thrombus size. However, both parameters are highly related to thrombus

topography at any given time.

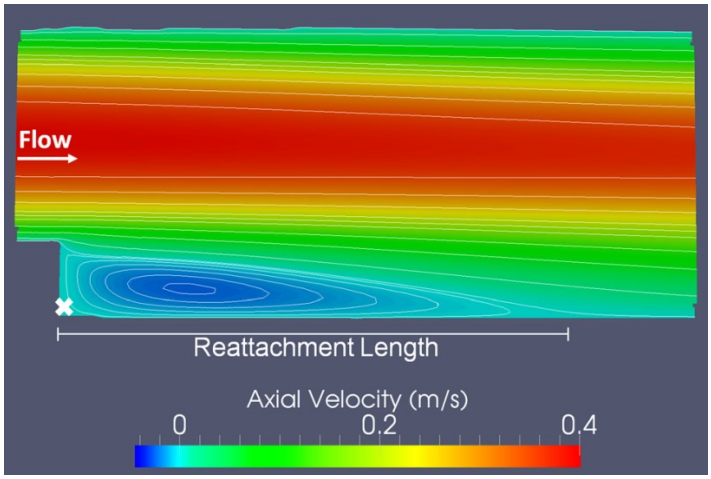


Figure 9 Contour of streamwise velocity from the CFD calculation of Joshua et al [15]. The blue region indicates the volume of the recirculation and the steady state reattachment length is 16.9 mm The bold white "x" is the location of the initiation of thrombus.

# Result and Discussion

## Simulation Setups

In this study, a series of 3D simulations are conducted for the backward facing step (BFS) in the circular pipe shown in figure 10 (a). The geometry is derived from the study of Joshua et al. 15). The model geometry is made by a commercial tool, ANSYS Design Modeler with a fine triangular mesh to resolve the step and curvature of the tube (figure 10. (a)(d)). The total length of the BFS model in the experiments is 12 (normalized by vessel diameter) along the z axis (from -2 to 10), but the computational domain is limited to 8 (from 0 to 8) in the consideration of saving computational time (Figure 10. (b)(c)). The step is located at 3 in z axis with a down stream distance 5 to minimize the outlet influence. The unshaded part of the vessel tube is obstacle.

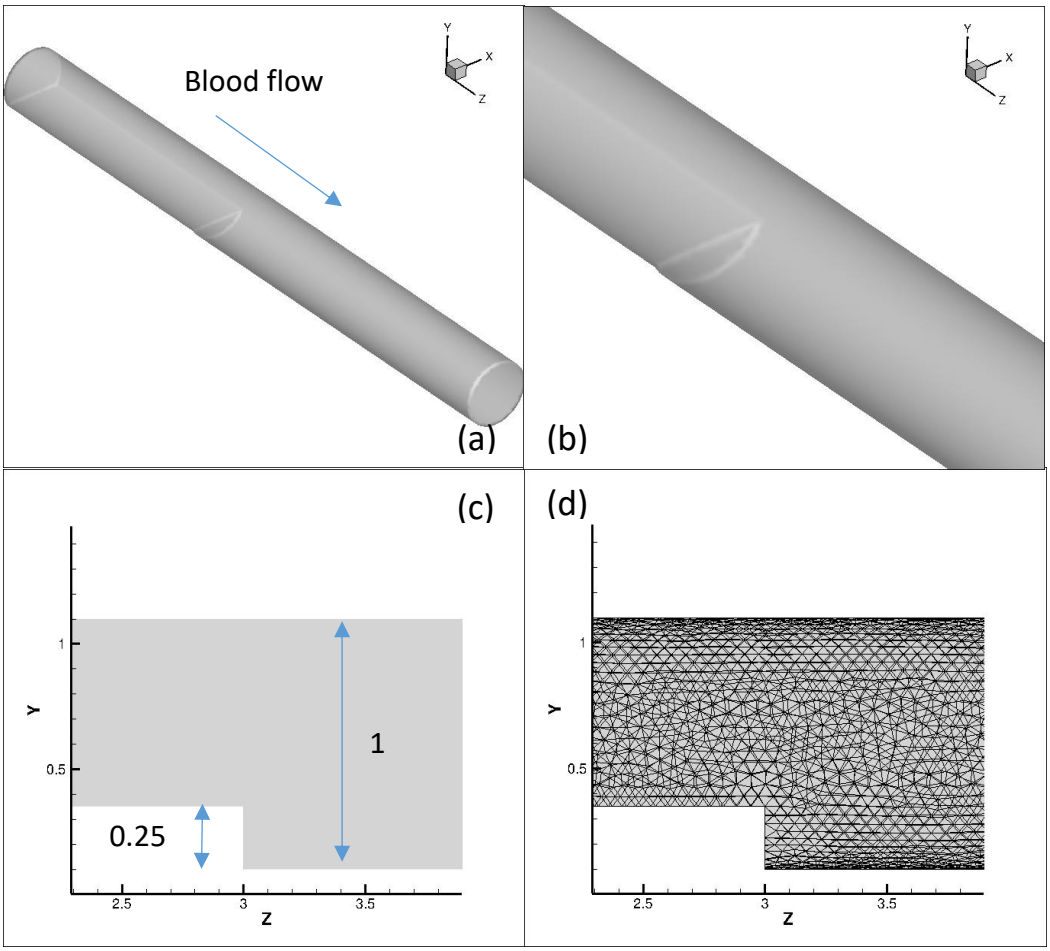


Figure 10 (a) A schematic view of the BFS model used in simulation. (b) Zoom in of BFS model. (c) Details of the step geometry: step height is 0.25, and z axis positon is 3. (d) Triangular mesh used to resolve the BFS model curvature and step geometry.

A uniform Cartesian grid is used to perform the simulations. The total number of cells is 64×64×256, in the x, y, and z directions respectively. Grid refinement is used to examine the effect of resolution on the results and the above mesh is found to be acceptable. The comparison for different grids will be described later in the next chapter.

Flow is arteries and veins is pulsatile. However, in the experiment, a steady flow generated by a peristaltic pump is used, and they minimize the pulsatility of the peristaltic pump by using a 4.0 m long tube. In the present simulations, we tested both steady flow as well as the flow with small

pulsatility at the inlet. The velocity profile at the inlet boundary is chosen to be uniform flow. i.e. $w$ is independent of $y$. For steady flow condition $w = 0.2\ m/s$ following Joshua et al, whereas for pulsatile flow condition $w = 0.2 + 0.05\sin(2\pi f t)\ m/s$ with choosing different frequencies. Thus the Re is the same based on the inlet hydraulic diameter, namely 490. A Neumann boundary condition for velocity is chosen at the outlet. The pressure has Neumann boundary conditions both at the inlet and the outlet.

## Simulation results

### Flow Field

Before presenting the simulation results about thrombus formation, we first performed flow field simulation and compared the results with the simulation done by Joshua et al.15). Once the flow reaches a steady state, we visualize the flow field and extract the stream wise velocity contour on the middle of yz-plane where the recirculation bubble shows its maximum length. Moreover, we perform simulations with perturbation on stream wise velocity as mentioned before to investigate the effect of small pulsatility that might be caused by the peristaltic pump:

$$w = 0.2 + 0.05\sin(2\pi f t)\ m/s \tag{32}$$

The volume of the recirculation bubble is indicated by the blue section located downstream of the step (at 3 on z-axis). However, the maximum length of recirculation bubble is around 12mm, which is off from the simulation done by Joshua et al. The stream wise velocity profile shows little change with perturbation, whereas the recirculation bubble size shrinks a little and backflow in the recirculation bubble is somewhat reduced. To check the effect of grid resolution on the recirculation bubble size, we performed another simulation with finer mesh.

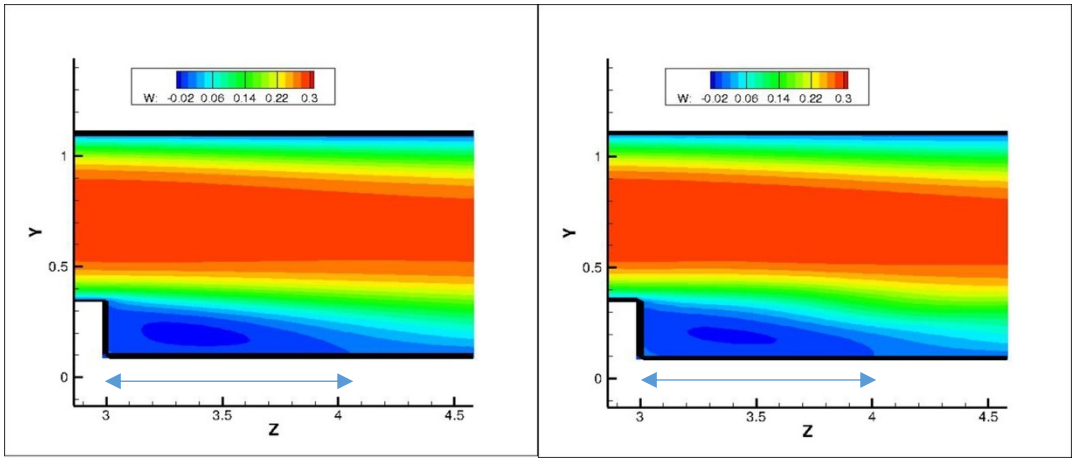


Figure 11 Stream wise velocity contour on middle yz-plane. The recirculation bubble shape is represented by blue section. The dark blue ellipse inside the bubble is where the backflow velocity is high. Left is flow field without perturbation and right is result with perturbation.

Instead of using 64×64×256 cells on x, y and z axis, we double the number of cells on each axis and the number of grid points now is 128×128×512. The recirculation bubble shape and streamwise velocity profiles are compared for the coarse and fine grids. From figure 12 we can see there is no significant difference in the bubble length and shape. Even quantitative comparison of stream wise velocity shows that the maximum difference is less than 5 %. Thus, the nominal mesh provides adequate resolution for these simulations.

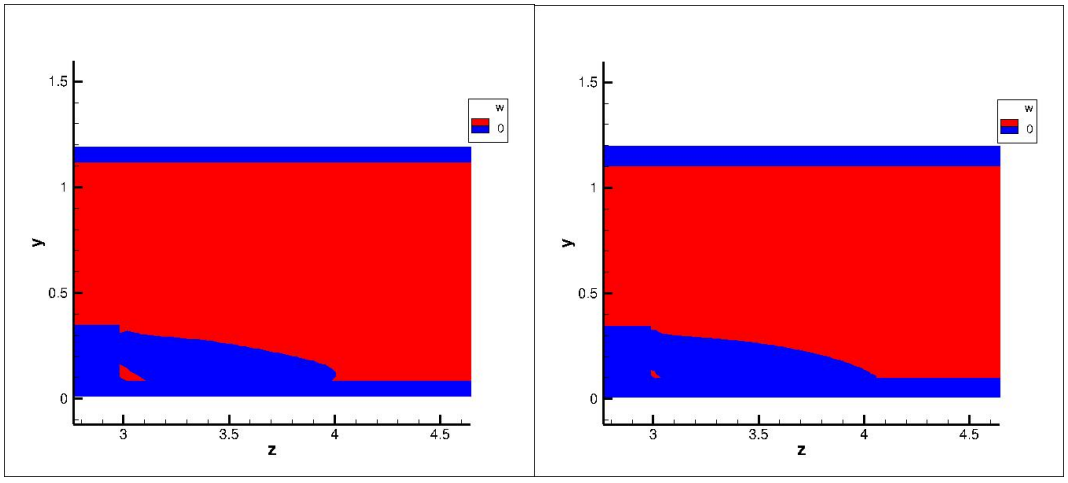


Figure 12 The zero velocity contour of streamwise velocity at the middle yz-plane. Left is the coarse grid and right is the fine grid respectively.

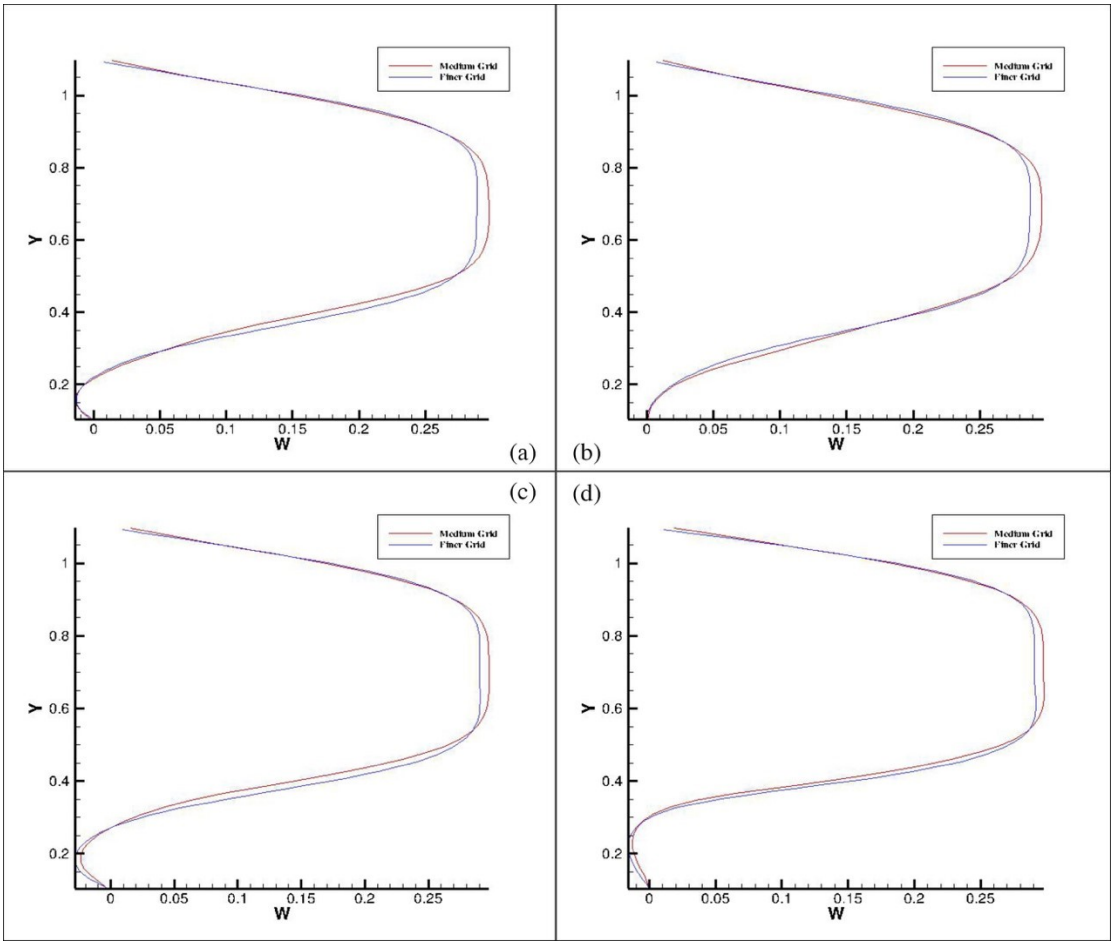

Figure 13 Comparison of stream wise velocity between coarse and fine grid. x-coordinate is the measurement of stream wise velocity and y-coordinate is y distance. Each pair of red and blue lines indicates represents velocity profile at different locations around the step on the middle yz-plane.

During the simulations, we adjust several key parameters because of the facts of: 1) there is no reference from other researchers' work, 2) the model we use is not exactly the same with previous ones such that we cannot directly adopt parameters. These key parameters includes: 1) $c^*$ in our model is the minimum concentration of thrombin that boosts platelets activation speed, 2) $A_{IIa}$ is the parameter controls the activation rate of inactivated platelet to activated platelet due to the presence of thrombin, 3) $k_{adh}$ controls adhesion rate of activated platelet to the wall, i.e. the converting of activated platelet to bounded platelet, 4) $k_{coh}$ controls the cohesion rate of activated platelet to other bounded platelet.

**Results from TF in Blood Volume**

The coagulation cascade is triggered by the exposure of damaged vessel wall to the blood stream. However, in the experiment done by Joshua et al, an acrylic BFS model is employed and there is therefore no TF exposure from the wall. In this scenario, one possibility is that the coagulation cascade may be triggered by the TF in the incoming blood flow. Thus the first series of simulation, for the TF, we set zero flux Neumann boundary condition on the BFS model wall and outlet, and Dirichlet boundary condition for the inlet, with a prescribe inlet concentration of TF. Simulations run for 100,000 time steps, which corresponds to 20s of real time. The resulting thrombus distribution and concentration are shown in figure below.

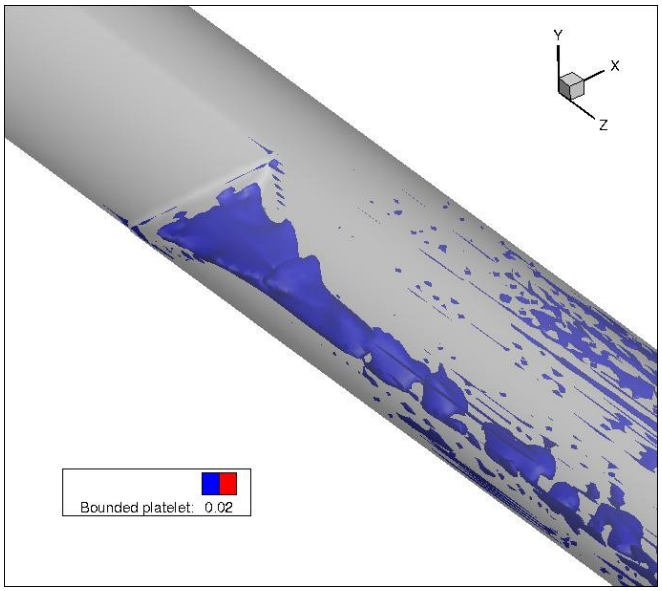


Figure 14 Thrombus visualized by bounded platelet (pTB) number density with iso-surface value 0.02, without perturbation.

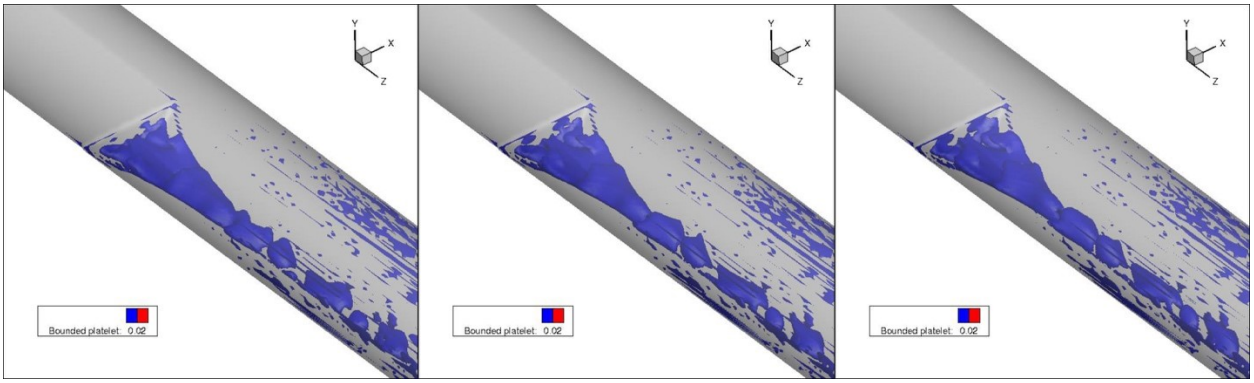


Figure 15 Thrombus visualized by bounded platelet (pTB) number density with iso-surface value 0.02. From left to right with perturbation frequency 5Hz, 10Hz, 20Hz.

The simulations are also performed with three different pulsatile frequencies: 5, 10, and 20Hz.The thrombus shapes in the recirculation bubble in the four configurations do not show any significant difference. At certain perturbation frequencies however, namely 0Hz and 10 Hz, the thrombus surfaces are smoother than that for the other cases. Thrombus formation in the computational model is not limited to the recirculation bubble and is also found to occur in some portions of the boundary layer where the streamwise velocity is low. However, because of the perturbation, the thrombii formed on the outer walls are to some degree washed away by the main flow. Figure 15 and 16 show with the same iso-surface value, the thrombus volume under perturbation is smaller than that without perturbation. As we focus on the relative high concentration of thrombus (0.022), fluid-phase chemicals in perturbed flow have higher chance to get through the recirculation bubble and subsequently boost the thrombus formation rate (figure 16. -18.). Although the thrombus concentration is low, higher growth rate comes with higher perturbation frequency.

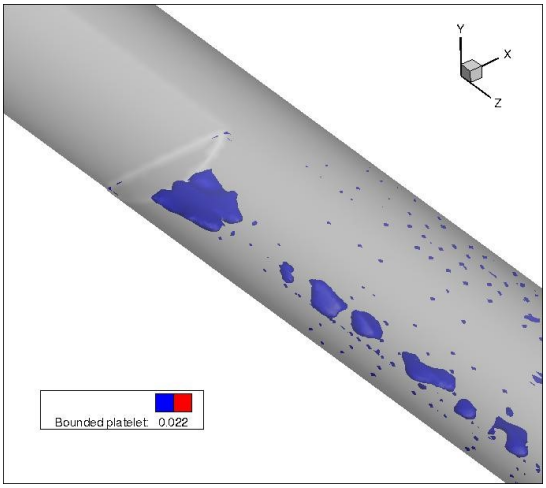


Figure 16 Thrombus visualized by bounded platelet (PTb) number density with iso-surface value 0.022 with perturbation frequency 5Hz.

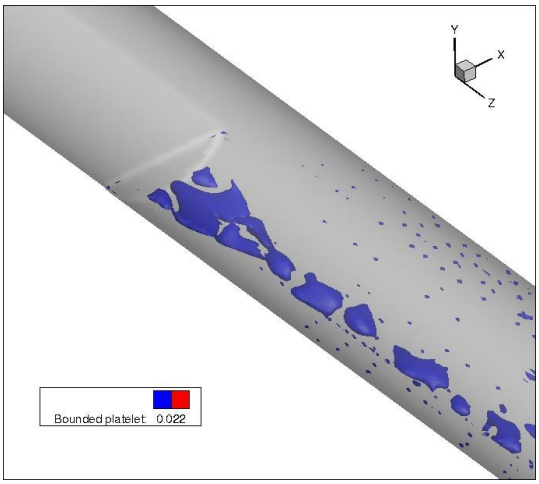


Figure 17 Thrombus visualized by bounded platelet (PTb) number density with iso-surface value 0.022 with perturbation frequency 10Hz.

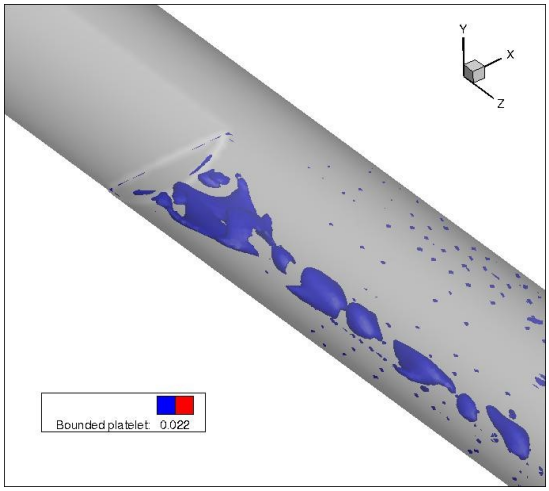


Figure 18 Thrombus visualized by bounded platelet (PTb) number density with iso-surface value 0.022 with perturbation frequency 20Hz.

We are also interested in the concentration and distribution of thrombin and residence time. Residence time (RT) is defined as the time for which the blood resides in a given region of interest. In previous study, RT is well correlated with thrombus distribution 5), thus we are interested in RT distribution and the correlation with thrombus distribution. Moreover, thrombin boosts the platelet activation rate, thus thrombin distribution is presumably associated with thrombus distribution.

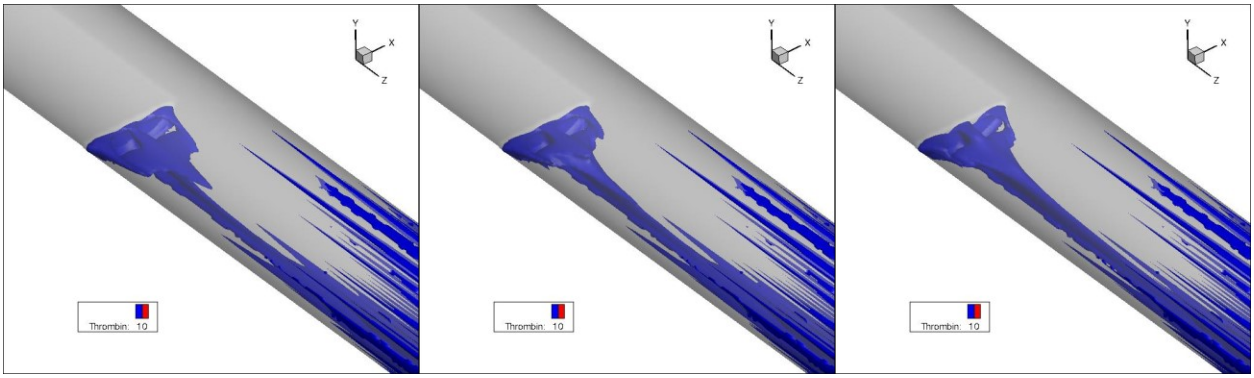


Figure 19 Thrombin distribution with iso-surface value 10. From left to right are the results of perturbation frequencies 5 Hz, 10Hz, and 20Hz.

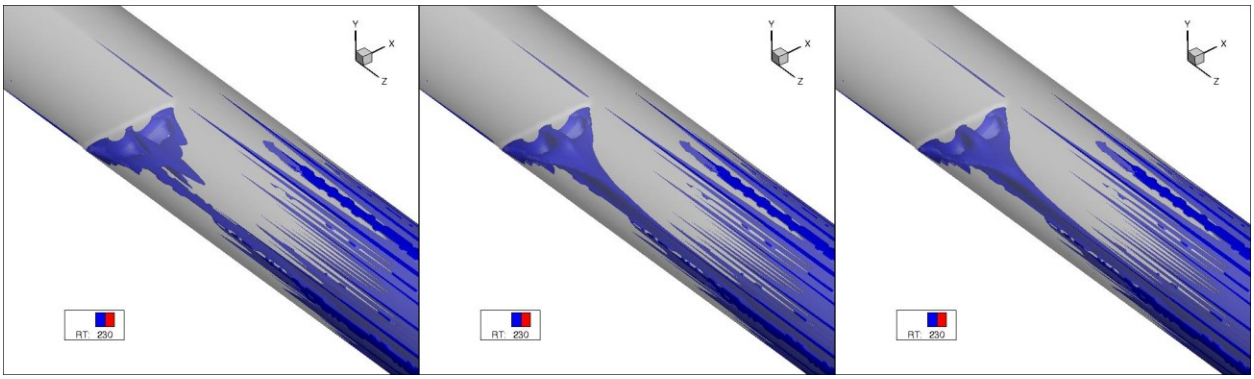


Figure 20 RT distribution with iso-surface value 50. From left to right are the results of perturbation frequencies 5 Hz, 10Hz, and 20Hz.

The shape of thrombin under different perturbation frequencies are similar except that fluid-phase chemicals are "mixed" better for higher frequencies and the iso-surfaces are somewhat smooth. The noteworthy aspect is that there are two obvious holes in the iso-surface bodies of thrombin and RT. This could be explained by following factors: 1) the flow field is symmetric about the center yz-plane (figure 22.) and it carries chemicals from two sides to the center then subsequently carries them downstream leaving little convection through the center yz-plane (figure 21.); 2) in the recirculation bubble region, the flow and has two separate circulation regions (figure 22.) on the two sides of center yz-plane and the absolute velocity is high in the two regions, which causes low RT and fluid-phase chemicals' concentration.

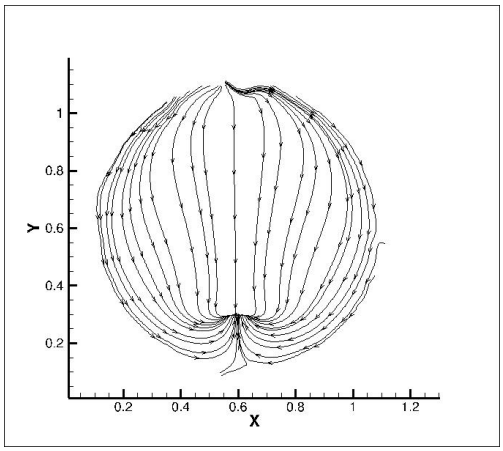


Figure 21 Stream lines on a k-plane section of recirculation bubble. Chemicals are carried by flow from two sides to the center.

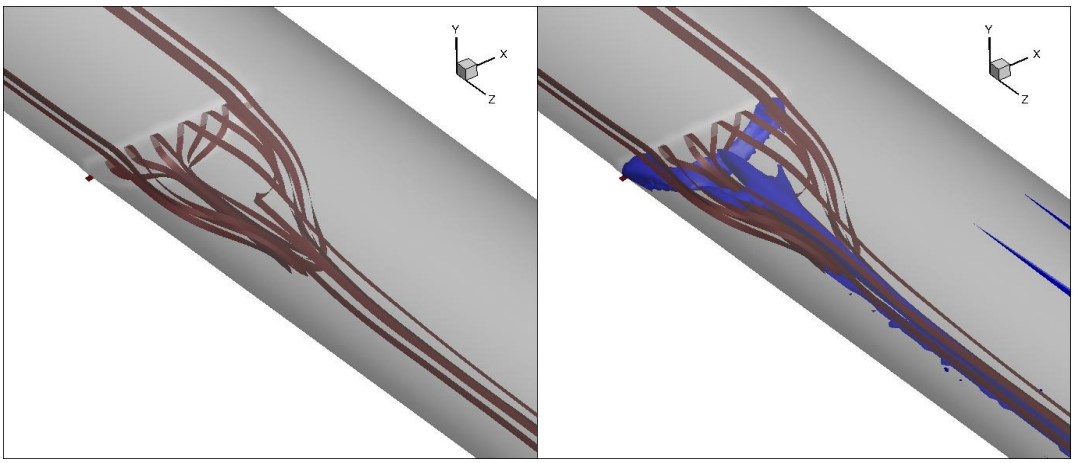

Figure 22 Left: 3D streamline in the region of recirculation bubble without perturbation. Clearly the recirculation bubble is divided into two regions. Right: the superimposing of thrombin iso-surface body with streamline. The two holes correspond with the two separate recirculation regions.

**Results from TF Wall Model**

The coagulation cascade is mainly triggered on the damaged wall where TF get exposed to the flow. In order to be consistent with the model, following simulations are run with TF Dirichlet boundary condition at the inner wall. Moreover, all previous simulation results show the magnitude of bound platelet number density of $1e-2$, which is too low and cannot be considered as "thrombus" at all. Factors like: 1) reaction rate, 2) blood volume TF assumption, 3) adhesion and cohesion rate, 4) iteration times are the keys to obtain desirable thrombus concentration. In the considerations of computational costs and simulation stability, here we first increase the TF concentration on the wall and extend simulation to 200,000 iteration times, which corresponding to 40s in real situation. First we test a situation where TF concentration goes extreme, say 1000 instead of 100.

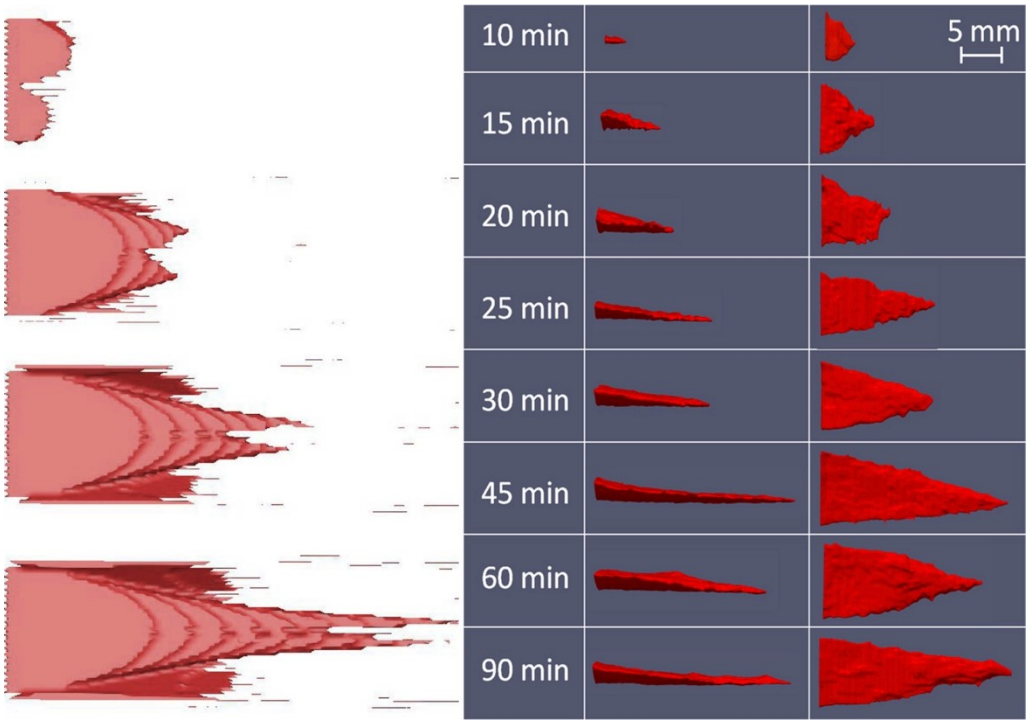


Figure 23 Top view of thrombus predicted by current model (left) and comparison with experimental results (right). From top to bottom are thrombus distribution with iso-surface value 0.95 at 108000, 112000, 116000, and 120000 iteration time step. These iteration time step correspond to 21.6s, 22.4s, 23.2s, and 24s in real situation.

In these simulation results, the thrombus length shows asymptotic growth pattern and reaches its maximum length around 120,000 iteration time step. The total length of thrombus is about 7 times the step height, which is almost the same with experimental results.

From the lateral view (figure. 24), the maximum thrombus height is almost the step height, while in experiment the maximum height is 0.98 times the step height. However, thrombus doesn't grow from the corner but from somewhere in the upper recirculation bubble and extend itself along the step surface to the downstream region. Moreover, there is a gap inside the thrombus, between the core and the upper part. As mentioned before, the core thrombus can be explained by the flow pattern in the recirculation bubble, in which the flow brings the chemicals to the center. The formation of suspended surface is because of the high boundary concentration: activated platelets

attach to the step edge and other activated platelets may attached themselves to bounded platelets and the sloped surface is formed under the influence of flow pattern.

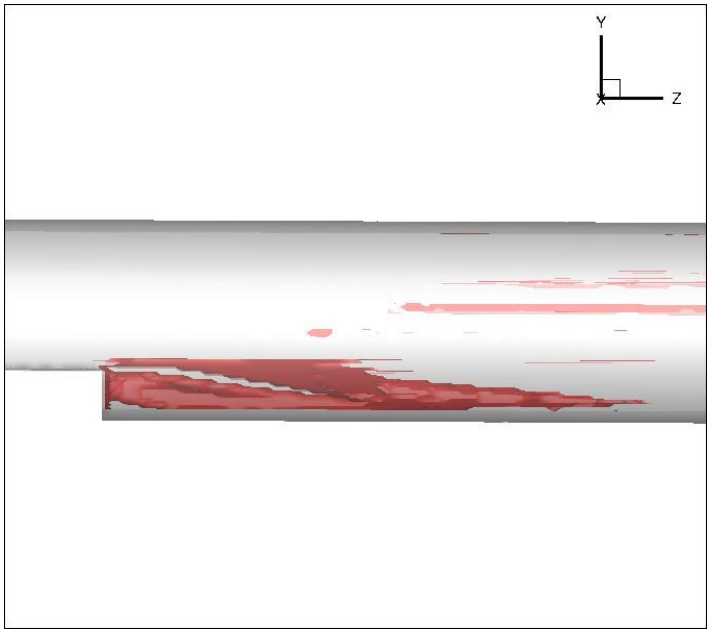


Figure 24 Lateral view of thrombus with maximum length 7 and height 1 (normalized by step height).

Obviously the initial TF boundary condition of a 1000 is unrealistic, but the main purpose of this simulation is to test whether the thrombus growth pattern is asymptotic. Increasing the initial TF concentration saves the computational as we get a thrombus iso-surface in 200,000 iteration time steps. At this stage we are curious about such a strange thrombus distribution is caused by the extreme TF boundary condition or intrinsically caused by our computational model. Therefore, we perform a simulation with 100 TF boundary and extend iteration time steps to 200,000. Not surprisingly, the final thrombus distribution is not much different from that from the simulation with 1000 TF boundary condition.

The same results from different TF boundary conditions reveal that the flow pattern is the key factor that controls the thrombus formation. This can also be illustrated by the distribution of

thrombin (T14) and RT (T19) (figure 25.). Unlike activated platelets, which are affected by adhesion and cohesion, fluid-phase chemicals are largely governed by the flow pattern. Thus, the distribution of these chemicals is highly correlated with RT. In the recirculation bubble the flow carries chemicals to the center and leaves two holes where the absolute velocity is high. Because of the high thrombin concentration in the center, platelet activation rate is high leading to the "core" thrombus formation. However, the suspended thrombus layer is not indicated by thrombin distribution. When we look at the early stage of thrombus growth, we find that the suspended layer always has higher thrombus concentration than in any other place in recirculation bubble (figure 26.). This is caused by two factors: 1) the extreme high TF boundary concentration, 2) the adhesion and cohesion model might be over simplified.

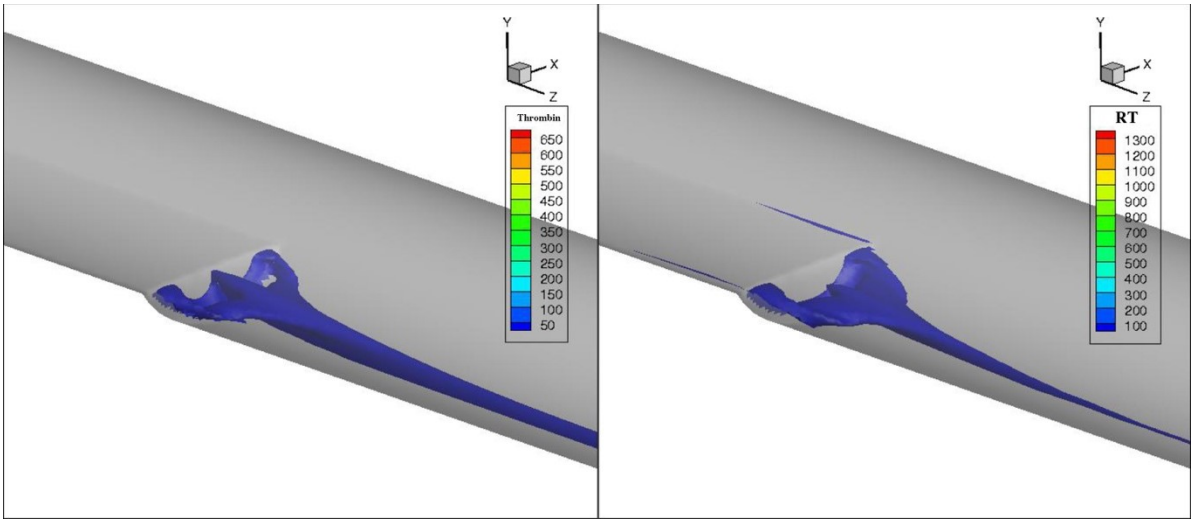


Figure 25 Left: Thrombin distribution with 1000 TF initial value, iso-surface value 50. Right: RT distribution with 1000 TF initial value, iso-surface value 100.

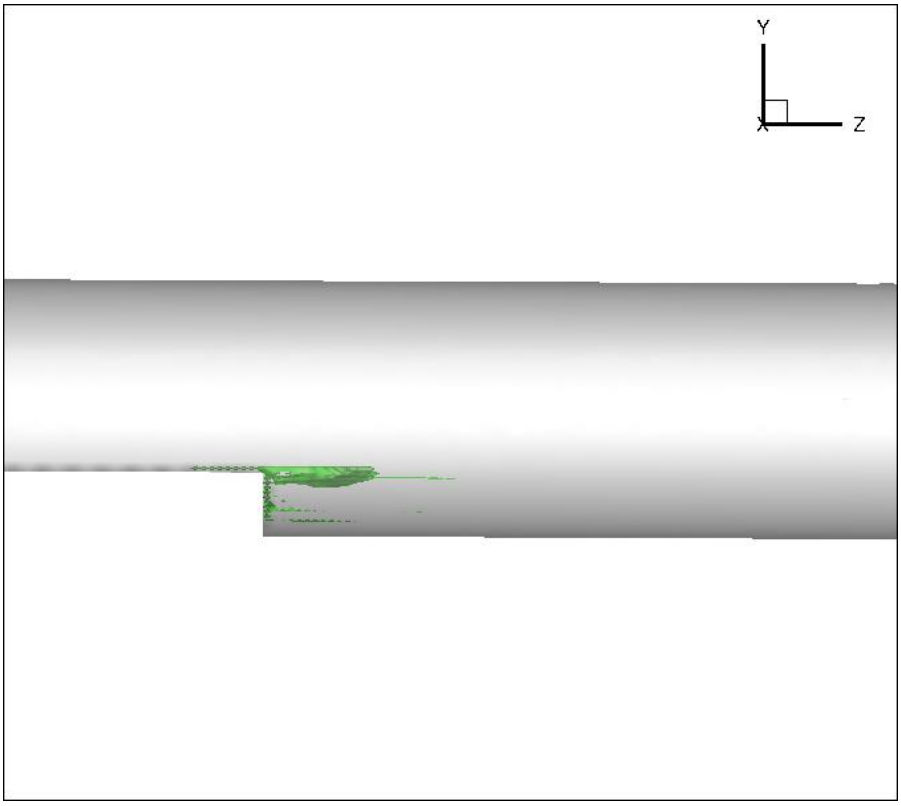


Figure 26 Lateral view of thrombus at 108000 iteration time step with iso-surface value 0.5.

**Function of Thrombin**

Detailed analysis of the thrombin distribution and concentration is important because it drives the platelet activation rate. In these simulation the TF boundary condition value is the primary variable and we employ values equal to 100 and 200. In this way, we can also investigate the influence of different TF boundary value on thrombin distribution and concentration.

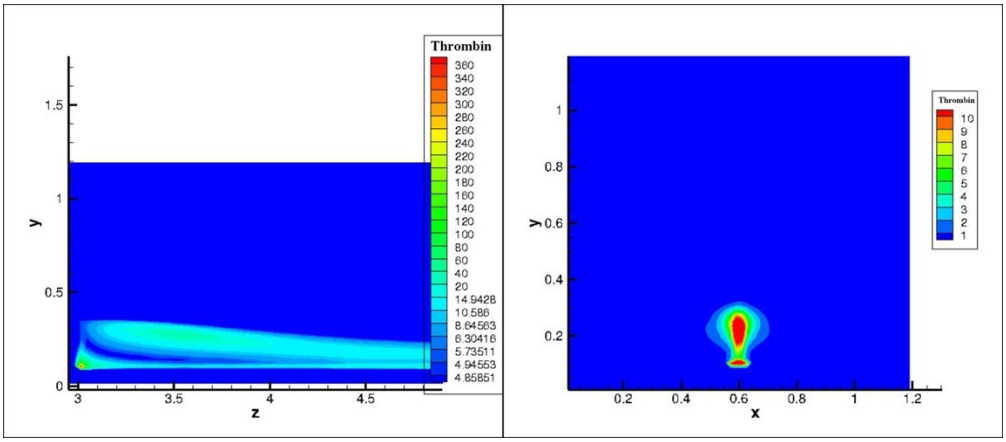


Figure 27 Left: Thrombin concentration contour on center yz-plane. Right: Thrombin concentration contour on one xy-plane inside recirculation bubble.

As evident from figure 28, both 100 and 200 TF boundary conditions show similar thrombin distribution and differences is concentration value. The highest thrombin concentration is located at the corner where it reaches a magnitude of $1e2$. Above the corner there is another region of relative high concentration of thrombin in the upper recirculation bubble, wherein the concentration reaches the magnitude of $1e1$. Such thrombin distribution can be explained by the stream line on xy-plane (figure 21.), in which the chemicals are carried to the upper recirculation bubble. We are also interested in the thrombin growth pattern at these two locations.

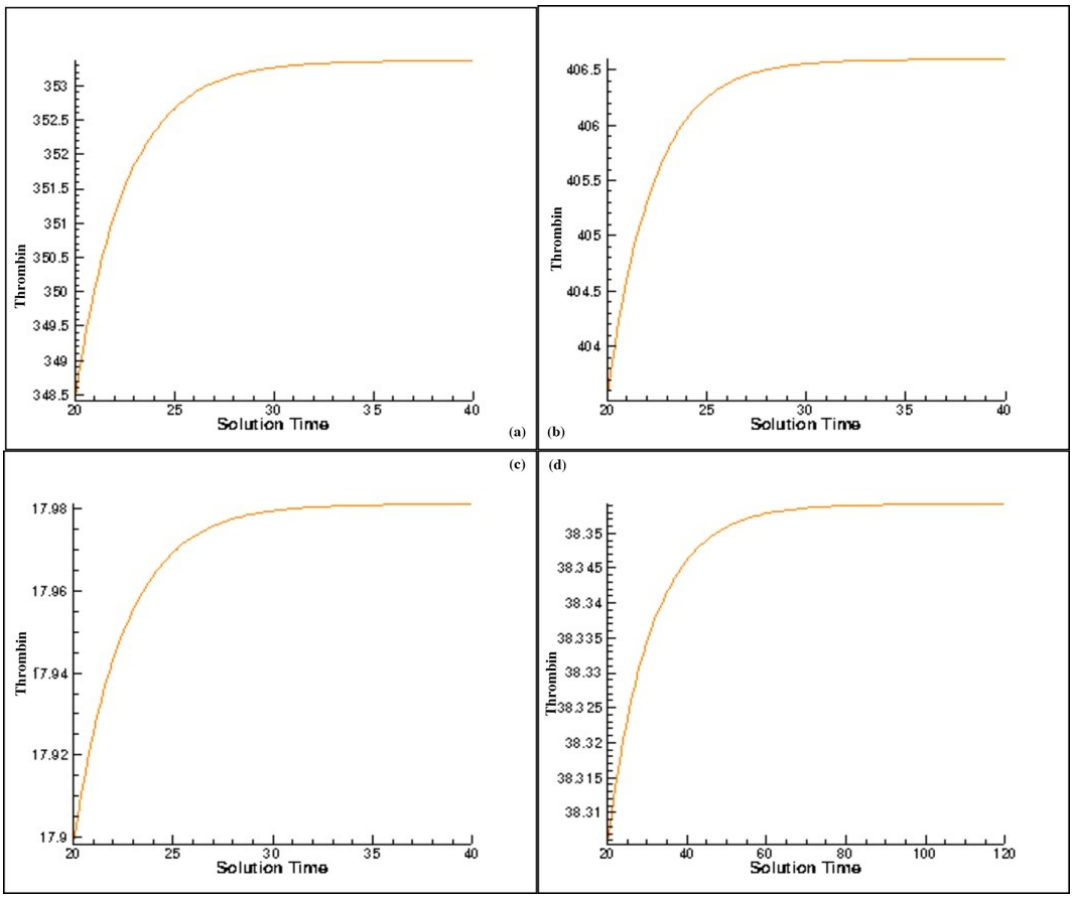


Figure 28 Thrombin growth pattern (a) at the corner with 100 TF boundary condition, (b) at the corner with 200 TF boundary condition, (c) in upper recirculation bubble with 100 TF boundary condition, (d) in upper recirculation bubble with 200 TF boundary condition.

At all location and for the different TF boundary condition, thrombin has an asymptotic growth pattern and reaches its maximum value almost at the same time. From the experimental results, thrombus start to grow from the corner. However, in the simulations thrombus grows from the suspended layer or from the "core". In order to focus thrombus formation in the corner, we adjust the parameter $c^*$ to 450 from its previous vale of 1 ($c^*$ is the minimum thrombin concentration that boost the platelet activation rate.). Moreover, we also increase the platelet activation rate $k_{IIa}$ by a factor of 10 to 0.05 to compensate for the increasing $c^*$, and lower the cohesion and adhesion rates to ensure the stability.

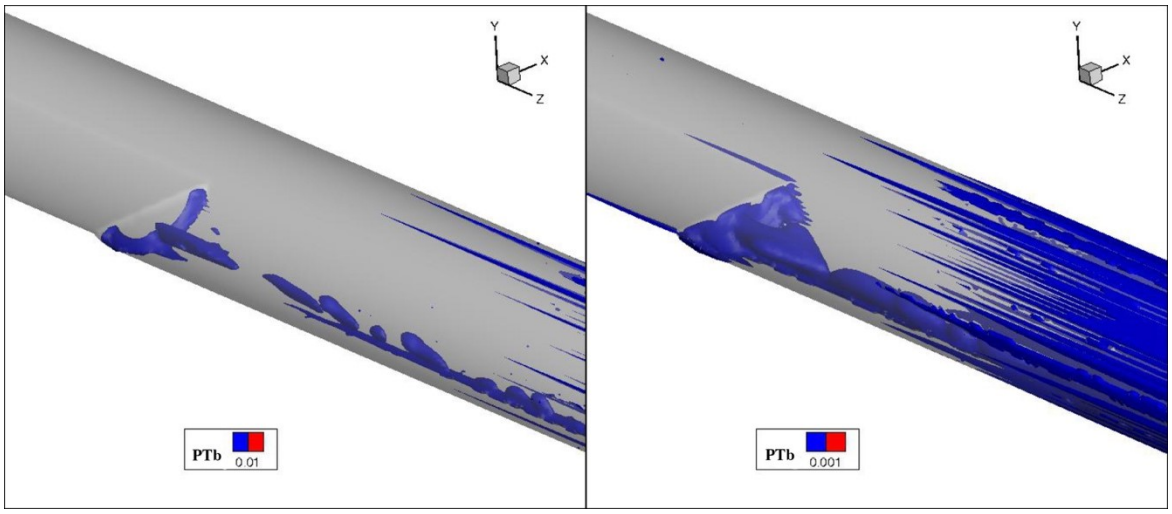


Figure 29 Thrombus visualized by bounded platelet (PTb) number density. Left: PTb number density iso-surface value 0.01. Right: PTb number density iso-surface value 0.001.

Clearly the overall thrombus concentration decreases because of the increase in $c^*$. However, compared with previous results (figure 23, 24.), thrombus growth is more limited to the corner, which is consistent with the experimental results. Due to the transport phenomenon, there is high thrombin concentration along the center line downstream. Similarly, the z-axial symmetric distribution of thrombus can be explained by no convection nor diffusion across the middle yz-plane. The thrombus distribution along the center line is quite interesting, and it is a result of platelet adhesion and cohesion. While looking into the contour of thrombin, the highest concentration is not located at the corner but somewhere downstream (figure 30.). The growth patterns (figure 31.) of 3 selected points reveal that: 1) thrombus start growing at a relative constant speed around the corner, 2) along the center line thrombus grows faster at a later time, 3) after a sharp increase the growth rates at upper recirculation bubble and downstream point decrease to the level slightly lower than that around corner.

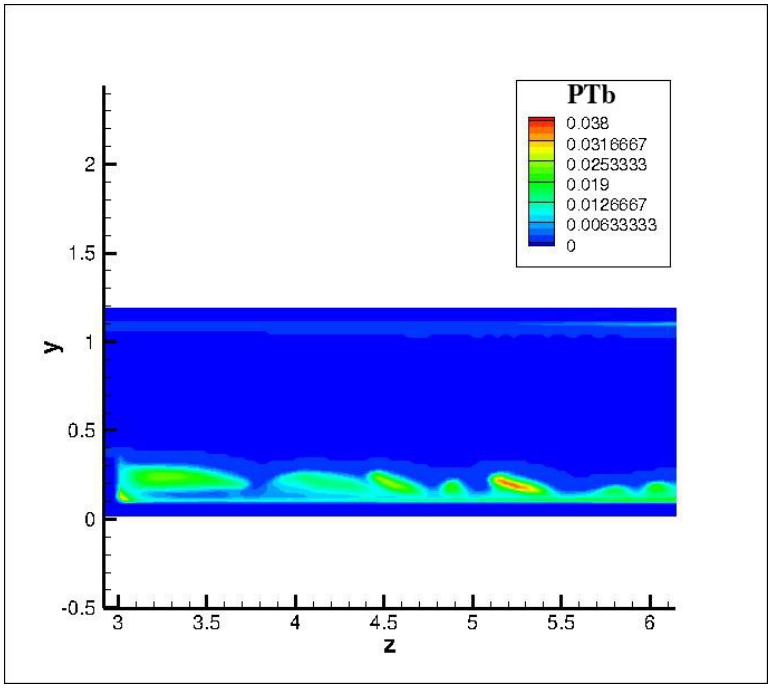


Figure 30 Bound platelet number density contour on center yz-plane with highest value 0.038 at somewhere downstream.

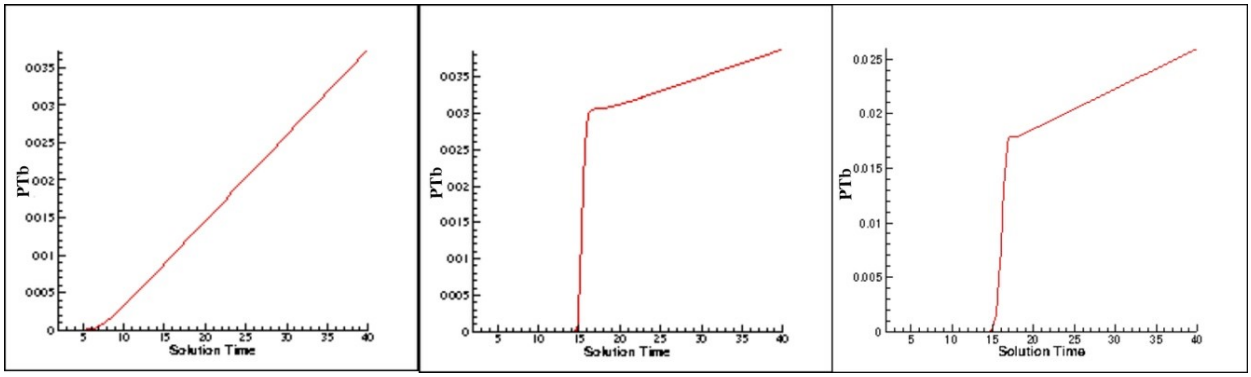


Figure 31 Bounded platelet growth pattern at different locations. From left to right: around the corner, highest concentration point along the center line, and upper recirculation bubble.

Again, because of the increase in $c^*$, the overall thrombin concentration decreases with the highest value of 510 occurring near the corner. A lower $c^*$ also changes the time for thrombin to reach its maximum value. it is worth noting that at 15s when thrombin reaches its maximum value, the thrombus concentration in the upper recirculation bubble and downstream point show a sudden increase. This is mainly caused by flow transport phenomenon: around 15s, thrombin

concentration around the corner is high enough to boost the platelet activation rate; activated platelets form in the recirculation bubble region and get transported downstream. It also means that activated platelets do not adhere or cohere locally in recirculation bubble region upon activation but are carried downstream along the center line.

We calculate the thrombus growth rate by subtracting thrombus concentration between two chosen time steps, namely the interval is 10,000 iteration time steps. By comparing the growth rate distribution (figure 34.), it is found that high growth rate is limited to the corner after 300,000 time steps.

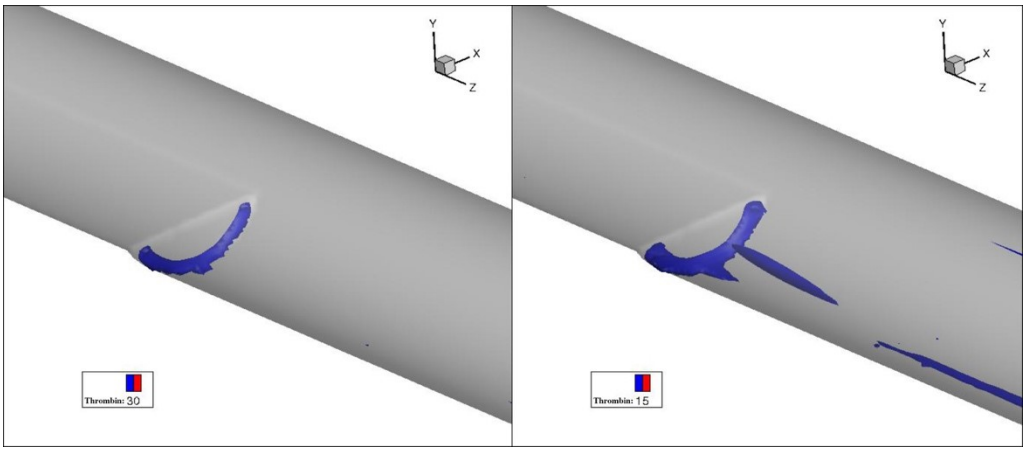


Figure 32 Left: thrombin distribution with iso-surface value 30. Right: Thrombin distribution with iso-surface value 15. Iteration time step 200,000.

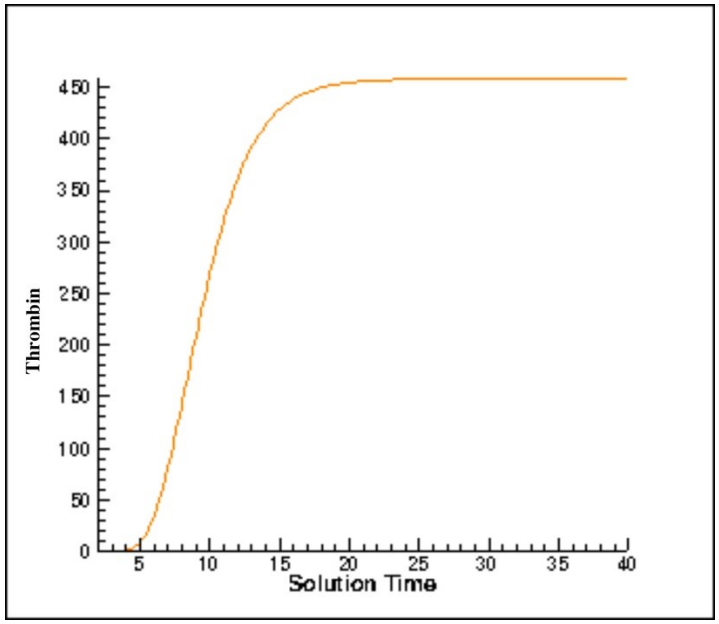


Figure 33 Thrombin growth pattern around the corner, reaching its max value around 15s.

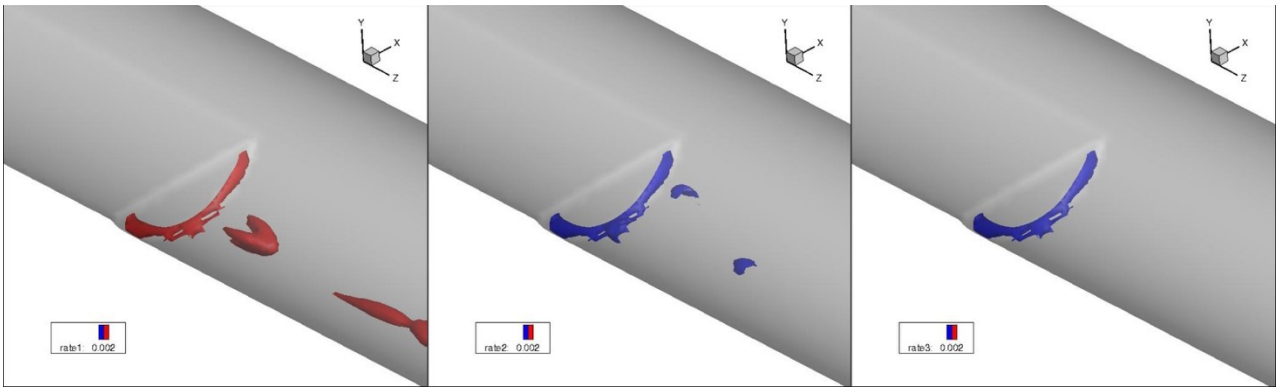


Figure 34 Thrombus growth rate distribution at 3 different time with iso-surface value 0.002. From left to right: 100,000, 200,000, and 300,000 iteration time steps.

Such growth rate distribution enables us to extrapolate the thrombus distribution because the growth rates are constants throughout the domain. The good aspect of such growth rate distribution is that high growth rate is located around the corner, but on the other hand the volume of high growth rate area is small. By extending the thrombus concentration to some value around 1, we get the iso-surface thrombus body (figure 35.). The formula used for extrapolation is:

$$C_f = C_1 + (C_1 - C_2)\Delta t, \tag{33}$$

where $C_f$ is the "reasonable" thrombus concentration we want, and $C_1, C_2$ are the successive PTb number density in time from simulation results, and $\Delta t$ is chosen to make $C_f$ reaching magnitude of 1.

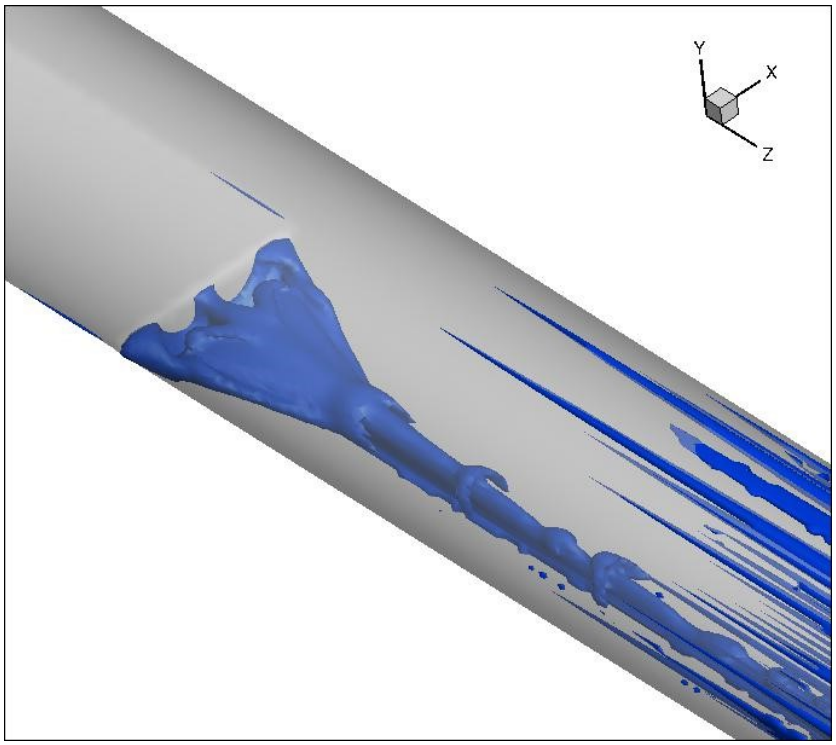


Figure 35 Final thrombus visualized by PTb number density extrapolation on time.

The general thrombus shape in figure 35 is similar to that observed in the experiments. The thrombus boundary converges to the center line along the z-axis, and the maximum height is almost the step height. However, because of the unchanged flow pattern, there are two holes in the recirculation bubble region due the high absolute velocity. The high concentration along the center line is due to two factors: 1) the TF boundary condition is not limited in recirculation bubble but all around the inner surface, 2) the flow carries chemicals toward center because of the symmetry about z-axis. Actually such thrombus distribution alone the center line would not occur in a

realistic situation since blood flow pattern in the human body is not perfectly symmetric and there is transportation and diffusion phenomenon along all directions. Furthermore, TF exposure only happens where the vessel wall is damaged.

**Penalty Force Model**

The most important factor that affects the coagulation cascade and thrombus formation is the flow pattern. In our simulation the flow pattern reaches its steady state before 10,000 iteration time steps and remains unaffected by the thrombus during the whole simulation. In reality, the thrombus and flow pattern are have a two-way coupled interaction: flow pattern leads to thrombus growth in certain locations and in turn the thrombus changes the flow pattern by exerting a frictional force and changing the geometry.

Given the porous nature of thrombus, the interaction mechanism is modeled by adding a force term proportional to the bound platelet number density into the governing equation. To test the penalty force model, we continue the simulation from 300,000 iteration time steps. First we choose the parameter $\phi_0^B$ ($\phi_0^B$ is the minimum bound platelet number density that penalty force model start working) in Eq.3 to be 3e-2 based on previous thrombus distribution (figure 36.).

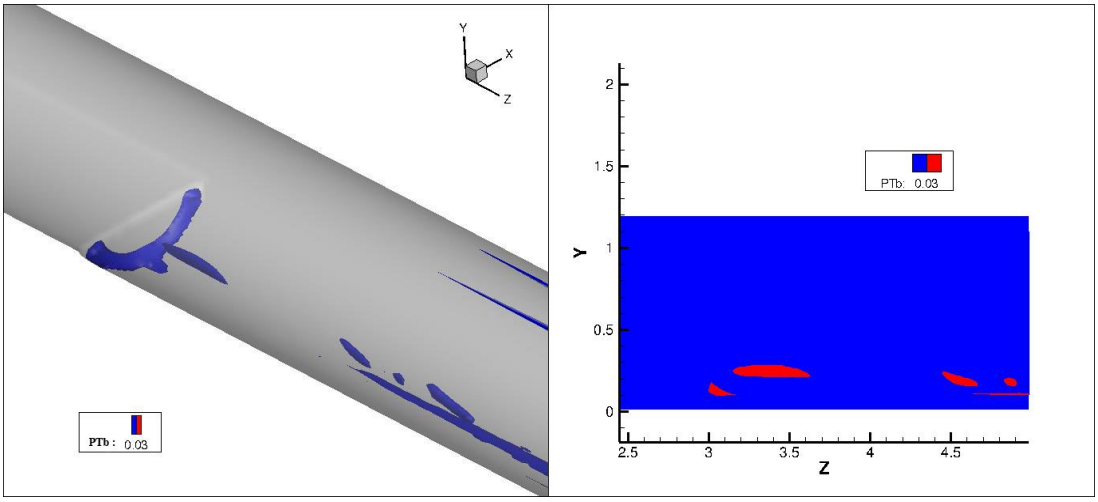


Figure 36 Left: Thrombus visualized by PTb number density with iso-surface value 0.03. Right: Lateral view of PTb with contour level 0.03 on the middle yz-plane. The iso-surface and contour of PTb indicate the part where penalty force is activated.

The reason for choosing $\phi_0^B$ to be 0.03 is to focus the thrombus formation in the recirculation bubble region especially around the corner. With the coupling term turned on, the simulation is continued for another 200,000 time-steps. Because there is no steady state for this coupled model, we examine the results after integrating for these 20000 time-steps to determine the effect of this coupling (figure 37.).

There are two major changes in the flow pattern: 1) the recirculation bubble length increases slightly in size and 2) the "stagnation area" (indicated by a black diamond) is thicker than that in . Looking back the thrombus distribution with iso-surface value 0.03, the penalty force model is activated around the corner and the core in upper recirculation bubble (figure 37.). Thus the flow pattern changes a little around the iso-surface.

In figure 38, the velocity profiles before and after the coupling are compares. We note that 1) before the step (figure 39(a)) and 2) the stream wise velocity does not change inside the

recirculation bubble, there is significant stagnation of the flow (figure 39(a)(b)), 3) the boundary layer become thicker and the main streamwise velocity is slightly higher than that in steady flow (figure 39. (d)).

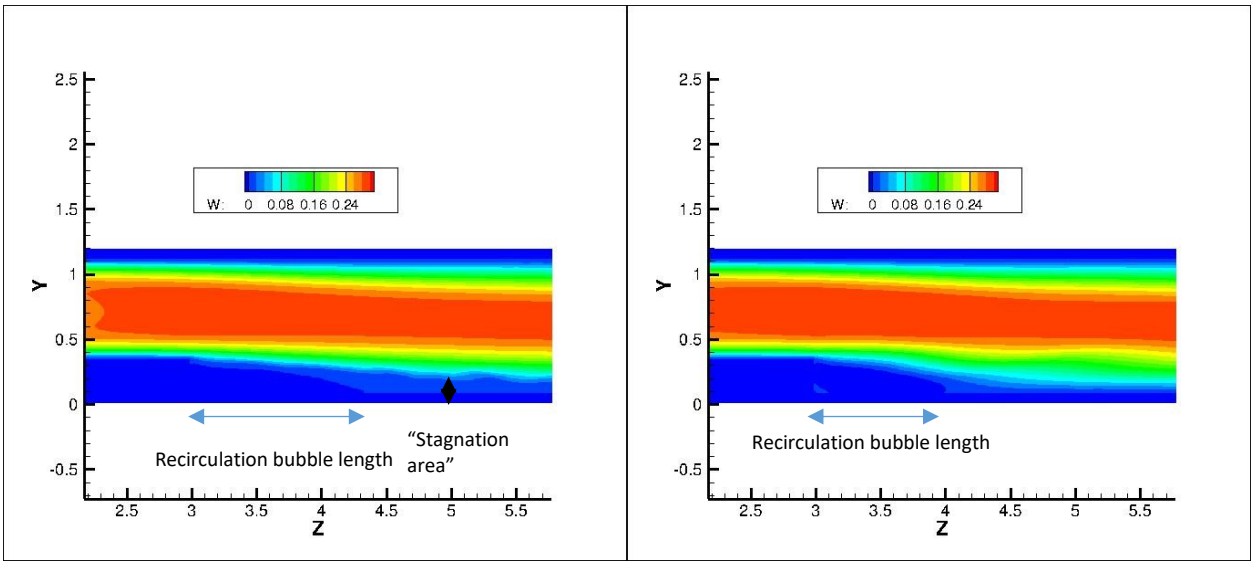


Figure 37 Stream wise velocity contour on the center yz-plane. Left: with penalty force model. Right: steady flow.

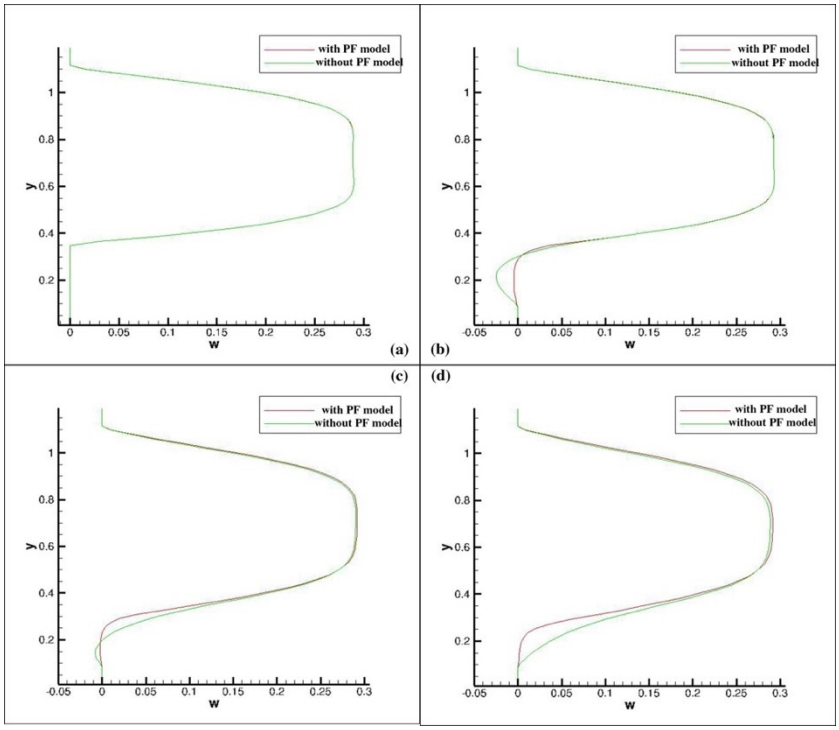


Figure 38 Stream wise velocity comparison along the center line at: (a) z=2.8mm, (b) z=3.2mm, (c) z=3.4mm, (d) z=4.4mm. x-axis is the velocity magnitude, and y-axis is the y direction.

The thrombus distribution is shown in figure 39. The thrombus shape is similar to that in the experiment. There are two obvious improvements: 1) the thrombus length extends to the same level with the experiment along z-axis, 2) thrombus grows from the corner and is well connected in the recirculation bubble. The total length is measured to be 18mm from the 2D lateral view with ignoring the downstream thrombus (figure 40.), whereas the experiment result is almost 25mm. However, for a higher thrombus iso-surface value shown in figure 41, we note that the thrombus is suspended over the recirculation bubble and below the thrombus surface there are two holes that are correlated with the stream line pattern.

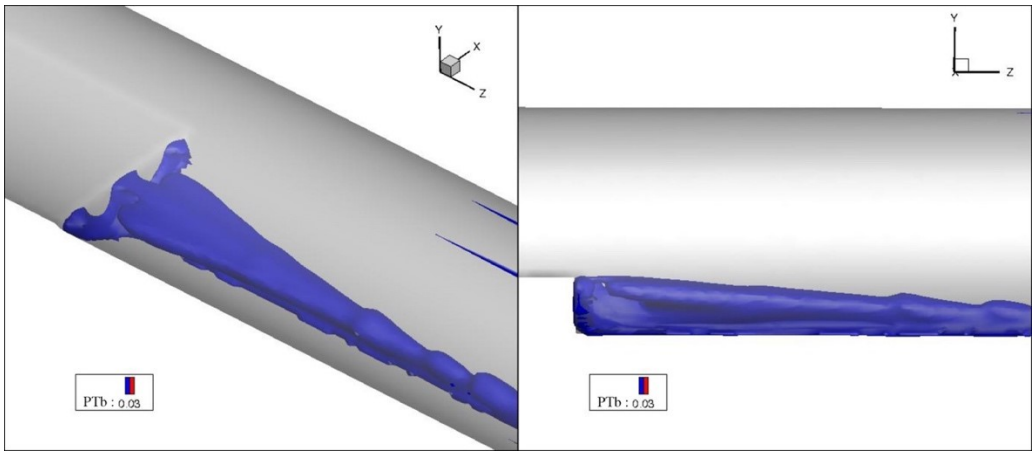


Figure 39 Thrombus visualized by PTb number density with iso-surface value 0.03. Right: lateral view.

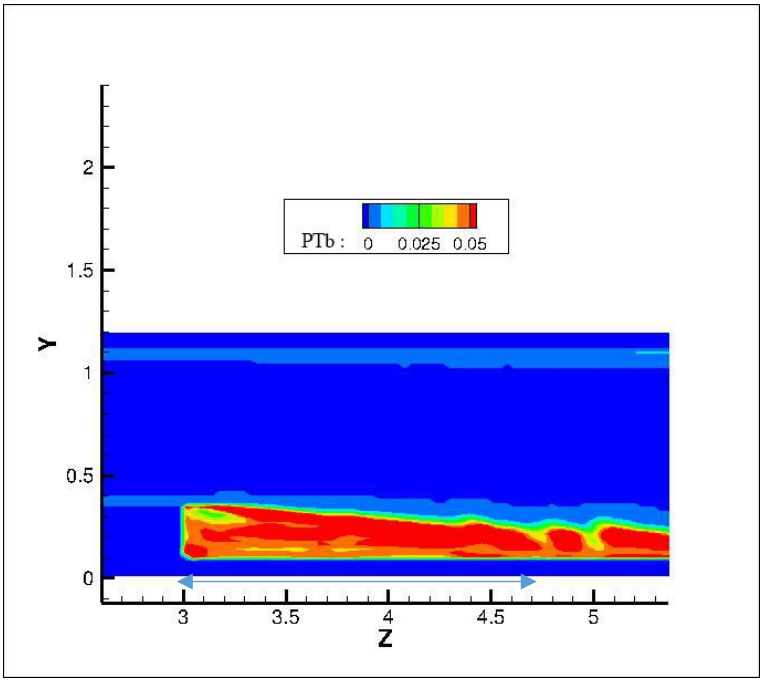


Figure 40 Thrombus concentration contour on the center yz-plane with measured thrombus length 18mm.

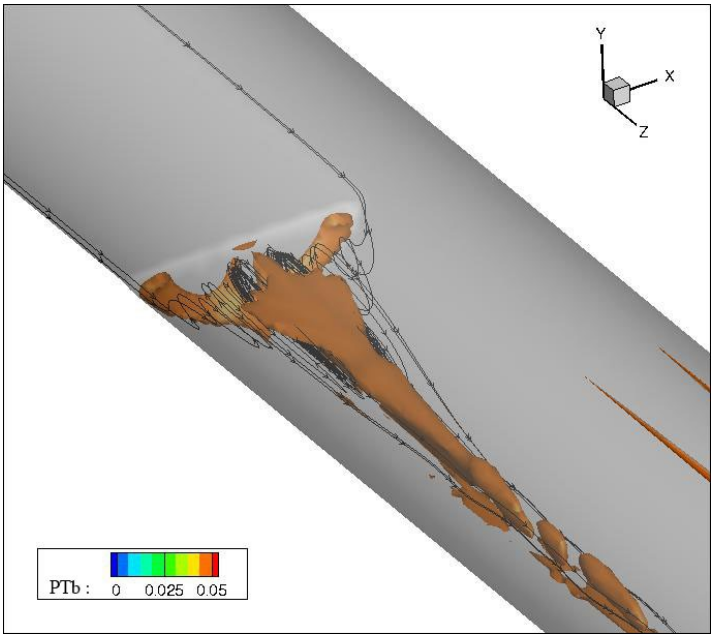


Figure 41 Thrombus visualized by PTb number density with iso-surface value 0.05, coupled with stream lines.

Because the thrombus volume with iso-surface value 0.03 is limited, the penalty force model activated only in a small region of the flow volume. With the initial thrombus distribution (see

figure 36), we observe thrombus growth both around the corner and in the core recirculation bubble region. But the symmetric nature of the flow pattern does not change and there are still two holes in that region. As the thrombus grows, the suspended surface will act as a barrier preventing chemicals transported into the recirculation bubble region.

However, the presence of the penalty force model changes the thrombin and RT distributions (figure 42), and we note that the two distributions no longer overlap as they did previously. Especially in the RT distribution, we note that there is no region of high concentration of RT in the recirculation bubble region. The distribution of thrombin is symmetric about the z-axis, and the main body of the thrombus is located the recirculation bubble region. From the streamline-thrombin coupled picture (figure 43), the thrombin volume almost perfectly matches the recirculation bubble. At this stage, the thrombin in the recirculation bubble region boosts the platelet activation of the suspended surface, which gives us the thrombus distribution in figure 41.

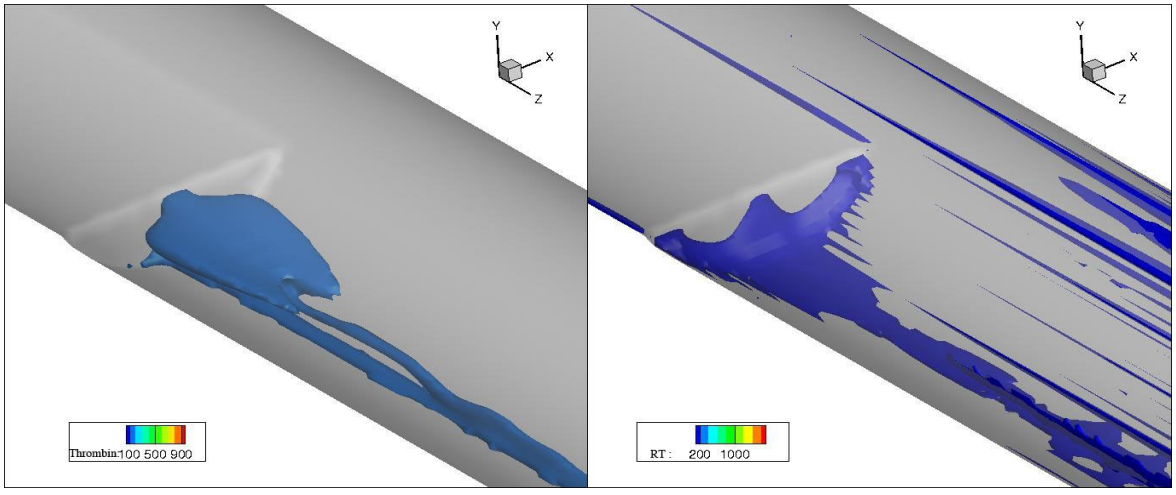


Figure 42 Left: thrombin distribution with iso-surface value 200. Right: RT distribution with iso-surface value 200.

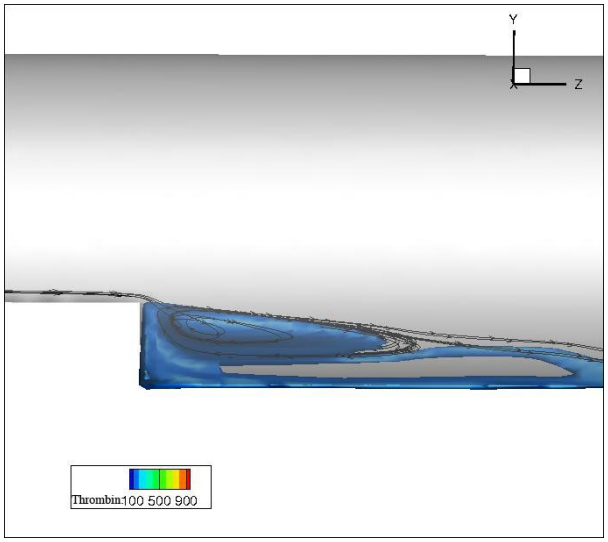


Figure 43 Streamline-thrombin coupled configuration, with thrombin iso-surface value 200.

# Conclusion

This study presents a computational model of thrombosis as well as its validation against experiments of Taylor et al. 15) that employ a simple backward facing step geometry . The chemo-fluidic coupled thrombosis computational model employed here is based on the work of Seo et al 5), which includes models for the coagulation cascade, platelet activation and fibrin polymerization. performed series of 3-D simulations have been performed to investigate both the flow field and chemical reactions. In order to match with the experiment, a variety of aspects of the simulation setup were modified including 1) boundary conditions for tissue factor; 2) initial flow profile; 3) key factors governing the coagulation cascade and platelet activation rate and 4) addition of a penalty force to model effect of thrombus on the flow.

The results show that the distribution and concentration of chemical factors are largely controlled by the flow patterns. In the simulation without the penalty force model, the flow pattern in the recirculation bubble shows that chemicals are carried from two sides to the center then transported

downstream by the main flow. Together with the fact that there is little transportation and diffusion across the center yz-plane there are actually two recirculation bubbles separated by the center yz-plane. In this situation, the distribution of residence time corresponds with the thrombin distribution, both leaving two holes in the recirculation bubble region. The distribution of thrombus (represent by bounded platelets) differs according to the presence of tissue factor. When the tissue factor is introduced in the flow volume, the thrombus surface is unsmooth and some parts protrude from the surface. When the tissue factor is exposed around the inner surface, there are two regions where the thrombus starts to grow, namely around the corner and the core in recirculation bubble region. Because the flow pattern in these simulations is not affected by the thrombus, the flow reaches a steady state that is independent of the thrombus geometry and the thrombus growth rate is determined by the steady state flow pattern. By extrapolating the thrombus concentration in time, we get the final thrombus distribution. The general shape of the resulting thrombus is similar with that of experiment result. However, due to the uneven thrombus grow rate in the recirculation bubble, the thrombus is full of "holes" that do not seem to exist in the experiments.

By adding a penalty force model into our model, the effect of the thrombus on the flow is considered. In the recirculation bubble region, the flow pattern is slowed down due to the stagnation effect of the thrombus. The distributions of thrombin and residence time have high concentration in the core and around the corner, which is unlike the previous results where thrombin and residence time correspond with each other. The high concentration of thrombin in the core region acting as an agonist boosts the platelet activation of the suspended surface (figure 41.). With lower iso-surface value, we can see the thrombus gradually fill the recirculation bubble from the core region and corner (figure 39.). The overall shape of thrombus is more similar with

experiment result than the previous simulation results. Even though the thrombus does not fill the recirculation bubble, it reaches height and length that are inline with the experimental result.

There are several limitations of the current study. First of all, we cannot run a simulation that matches the total real time of the experiment experiment. This is also the main reason the thrombus concentration is low throughout our simulations. Second, our integrated model is not as complete as the combination of three models from previous studies 6)13)14). The simplification may cause inaccurate chemical reaction results. Third, the blood flow profile in human artery is closer to a Womersley profile created by a fluctuating pressure drop through the artery whereas in our study we use Poiseuille flow profile corresponding to the steady state. Additionally, in previous studies, the thrombus made up of a mixture of fibrin and bound platelet, whereas in our study, we represent the thrombus by bound platelets only and omit the interaction between platelets and fibrin. Later studies could focus on addressing on these problems.

# References

**1)** Furie, K. L. et al., Guidelines for the prevention of stroke in patients with stroke or transient ischemic attack: a guideline for healthcare professionals from the American heart association/American stroke association, Stroke, 2011, 42(1):227-76.

**2)** Stoll Guido, Christoph Kleinschnitz, and Bernhard Nieswandt, "Molecular mechanisms of thrombus formation in ischemic stroke: novel insights and targets for treatment." Blood 112.9 (2008): 3555-3562. Web. 29 Jan. 2017.

**3)** Feigin, V. L., Lawes, C. M., Bennet, D. A., Anderson, C. S., Stroke epidemiology: a review of population-based studies of incidence, prevalence, and case-fatality in the late 20th century. Lancet Neurol2003; 2:43-53.

**4)** Bruce, Furie, Barbara, C. Furie, Mechanisms for thrombus formation. N Engl J Med 2008; 359:938-949

**5)** Jung-Hee Seo et al, A coupled Chemo-Fluidic Computational Model for Thrombogensis in Infarcted Left Ventricles. American Journal of Physiology-Heart and Circulatory Physiology (2016): ajpheart-00855.

**6)** Leiderman, K. and Fogelson, A. L., Grow with the flow: a spatial-temporal model of platelet deposition and blood coagulation under flow. Math. Med. Biol. 28: 1: 47-84, 2011.

**7)** Dubois, C., Panicot-Dubois, L., Gainor, J. F., Furie, B. Thrombin-initiated platelet activation in vivo is vWF independent during thrombus formation in a laser injury model. J. Clin. Invest. 2007: 117: 953-960

**8)** Dubois, C., Panicot-Dubois L, Merrill-Skoloff G, Furie, B., Furie, B. C., Glycoprotein VI-Dependent and – independent pathways of thrombus formation in vivo. Blood 2006: 107: 3902-3906.

**9)** Ruggeri, Z. M., Old concepts and new developments in the study of platelet aggregation. J. Clin. Invest. 2000: 105: 699-701.

**10)** Bluestin, D., Niu, L., Schoephoerster, R. T., and Dewanjee, M. K., 1996, "Steady Flow in an Aneurysm Model: Correlation Between Fluid Dynamics and Blood Platelet Deposition," ASME J. Biomech Eng, 118(3), pp. 280-286.

**11)** Karino, T., and Goldsmith, H. L., 1979, "Aggregation of Human Platelets in an Annular Vortex Distal to a Tubular Expansion," Microvasc. Res., 17(3), pp. 217-237.

**12)** Jones, K.C., and Mann, K. G. (1994). A model for the tissue factor pathway to thrombin. II. A mathematical simulation. J. Biol.Chem. 269, 23367-23373.

**13)** Biasetti, J., Spazzini, P. G., Swedenborg, J. and Gasser, T. C., An integrated fluid-chemical model toward modeling the formation of intra-luminal thrombus in abdominal aortic aneurysms. Front Physiol. 3: 266, 2012.

**14)** Neeves, K., Illing, D., and Diamond, S., Thrombin flux and wall shear rate regulate fibrin fiber deposition state during polymerization under flow. Biophys. J. 98: 7: 1344-1352, 2010.

**15)** Taylor, Joshua O. et al., "In vitro quantification of time dependent thrombus size using magnetic resonance imaging and computational simulations of thrombus surface shear stresses." Journal of biomechanical engineering 136.7 (2014): 071012.

**16)** R. Mittal et al., "A versatile sharp interface immersed boundary method for incompressible flows with complex boundaries," Journal of Computational Physics, vol. 227, pp. 4825-52, 2008.

**17)** W. H. Press, B.P. Flannery, S.A. Teukolsky, W.T. Vetterling, Numerical Recipes in Fortran, Cambridge University Press, 1992.

**18)** Beaudoin, J. F., Cadot, O., Aider, J. L., and Wesfreid, J. E., 2004, "Three-Dimensional Stationary Flow Over a Backward-Facing Step," Eur. J. Mech. B, 23(1), pp. 147-155.

**19)** Williams, P. T., and Baker, A. J., 1997, "Numercial Simulations of Laminar Flow Over a 3D Backward-Facing Step," Int. J. Numer. Methods Fluids, 24(11), pp. 1159-1183.

**20)** Armaly, B. F., Durst, F., Pereira, J. C. F., and Schonung, B., 1983, "Experimental and Theoretical Investigation of Backward-Facing Step Flow," J. Fluid. Mech., 127, 99. 473-496.

**21)** Kuharsky, A. L. & Fogesel A. L., (2001) Surface-mediated control of blood coagulation: the role of binding site densities and platelet deposition. Biophys. J., 80, 1050-1074.

**22)** Harfi Thura T., Seo Jung-hee, Yasir Hayder S., Welsh Nathaniel, Mayer Susan, Abraham Theodore P., George Richard T., Mittal Rajat, "The E-Wave Propogation Index (EPI): A Novel Echocardiographic Parameter for Prediction of Left Ventricular Thrombus. Derivation from Computational Fluid Dynamic Modeling and Validation on Human Subjects", International Journal of Cardiology (2016), doi:10.1016/j.ijcard.2016.10.

# Curriculum Vitae


## Ge Yan

**Address: 500 W University Parkway, Baltimore, MD 21210**

**Tel: 443-447-5757**

**E-mail: gyan6@jhu.edu**


## EDUCATION

**South China University of Technology** Sept.2011-Jun.2015
Bachelor's Degree in Thermal Energy and Power Engineering Overall GPA: 3.45 Major GPA: 3.80
**The Johns Hopkins University** Aug.2015-Now
Master Degree in Mechanical Engineering, majoring in Fluid Mechanics
Highlighted courses: Fluid Dynamics I and II, Computational Fluid Dynamics, Advanced Mathematical Methods for Engineer

## MAIN RESEARCH EXPERIENCE

**Fluid Physical and Computational Lab, Johns Hopkins University** Mar.2016-Now
**Research assistant**
- Developed Penalty Force Model in Vicar3d CFD program.
- Designed and conducted 3D-simulations about blood passing stent to analyze several chemical reaction processes.
- Conducted simulations about thrombosis process in BFS model, analyzing results and determining crucial parameters.
- Collaborated with fellow graduate students in Vicar3d code maintenance, conducting code test and debugging.

**Guangdong Province Key Laboratory of Efficient and Clean Energy Utilization,**
*South China University of technology, China* Jun.2014-Sep.2014
Researcher for The online measurement of heavy mental in PM 2.5 by Dual-pulse laser-induced breakdown spectroscopy

- Collected and read relevant research papers for reference.
- Built experiment base and assembled equipment. Conducted experiments and collected data.
- Collaborated and coordinated with faculty, staff scientists, and graduate students.

**Refrigeration Technology Curriculum Design, Dual-Phase Cooling Refrigeration System**
Nov.2013
- Led the entire group designing job and assigned work to group members.
- Designed the system and calculated the parameters given the cooling capacity.
- Designed the worked sheet and connected every parameter with macro, making it an auto-design program.

## INTERSHIP

**Teaching Assistant Introduction to Fluids Mechanics Lab** Sept. 2016-Dec. 2016
*Whiting School of Engineer, The Johns Hopkins University*
- Prepared lectures and guided undergraduate students doing scheduled experiments.
- Answered students' question regarding fluid mechanics and graded their lab reports and problem sets.

**Intern Qinling Mountains Power Plant** Jan.2014-Mar.2014
- Worked as an assistant operator to monitor the data and participated in daily inspection.
- Took apart in the Plant Safety Accession and Education activities.

**Intern JDC Molybdenum Group Co., Ltd. Heating Supply Dept.** June.2013-Aug.2013
- Assisted in the annual overhaul in summer. data processing of the boiler system.
- Processed data in failure analysis and assisted in replacing invalid parts of the boiler.

## MAIN SCHOLARSHIP&HONORS

2013-2014: The First Prize Scholarship
2012-2013: Merit Student of South China University of Technology
2012-2013: The Second Prize Scholarship